Moderní témata ve fyzice kondenzovaných látek

- fundamentální problémy chování hmoty, rozmanitost a překvapivé objevy s frekvencí typicky ne menší než

$$3.2\times10^{-8}\ s^{-1}$$

- aplikace, zejména komunikační technologie

Moderní témata ve fyzice kondenzovaných látek

- fundamentální problémy chování hmoty, rozmanitost a překvapivé objevy s frekvencí typicky ne menší než 1/rok
- aplikace, zejména komunikační technologie

Obsah této části „Moderních témat“:

- Frekvence Nobelových cen (NP) za fyziku kondenzovaných látek
- Vizualizace až do atomárních rozměrů – STM, AFM (NP 1986)
- Ukázka nízkorozměrných polovodičových struktur (několik NP, zejména 1985 – kvantový HE)
- Magnetorezistence v kovových nanostrukturách (NP 2007)
- Grafén (NP 2011)

Ukončení kursu:

výběr tématu (po dohodě s některým s přednášejících) pro písemné zpracování,

odevzdat do konce zkouškového období .

http://nobelprize.org/physics/laureates/index.html

2018 Ashkin, Mourou, Strickland (laserová fyzika, generace intenzivních ultrakrátkých pulsů)

2016 Thouless, Haldane, Kosterlitz (Topologické fázové přechody a topologické fáze hmoty)

2014 Akasaki, Amano, Nakamura (modré-UV světlo z polovodičových LED)

2011 Andre Geim, Konstantin Novoselov (grafén)

2009 Charles K. Kao (optická vlákna), W.S. Boyle, G.E. Smith (CCD)

2007 Albert Fert, Peter Gruenberg – objev Gigantické magnetorezistence

2003 Alexei A. Abrikosov, Vitaly L. Ginzburg, Anthony J. Leggett – teorie supravodivosti a supratekutosti

2001 Eric A. Cornell, Wolfgang Ketterle, Carl E. Wieman – Boze-Einsteinova kondenzace

2000 Zhores I. Alferov, Herbert Kroemer, Jack S. Kilby – základy komunikačních a informačních technologií

1998 Robert B. Laughlin, Horst L. Störmer, Daniel C. Tsui – objev kvantové kapaliny se zlomkově nabitými excitacemi

1996 David M. Lee, Douglas D. Osheroff, Robert C. Richardson – objev supratekutosti v He3

1994 Bertram N. Brockhouse, Clifford G. Shull – pionýrský příspěvek k metodám neutronového rozptylu v kond. l.

1991 Pierre-Gilles de Gennes – metody popisu kapalných krystalů a polymerů

1987 J. Georg Bednorz, K. Alex Müller – objev vysokoteplotní supravodivosti

1986 Ernst Ruska, Gerd Binnig, Heinrich Rohrer – elektronový mikroskop, STM

1985 Klaus von Klitzing - kvantový Hallův jev

2014 – mezinárodní rok krystalografie

1914 Max von Laue – rtg difrakce na krystalech
1915 W.H. Bragg & W.L. Bragg, dtto

2015 – mezinárodní rok světla

2014 Akasaki, Amano, Nakamura (modré-UV světlo z polovodičových LED)

Makroskopické,
mikroskopické,
nanometrové
rozměry

1 m
=
10^3 mm
=
10^6 μm
=
10^9 nm

= 10^{12} pm
= 10^{15} fm

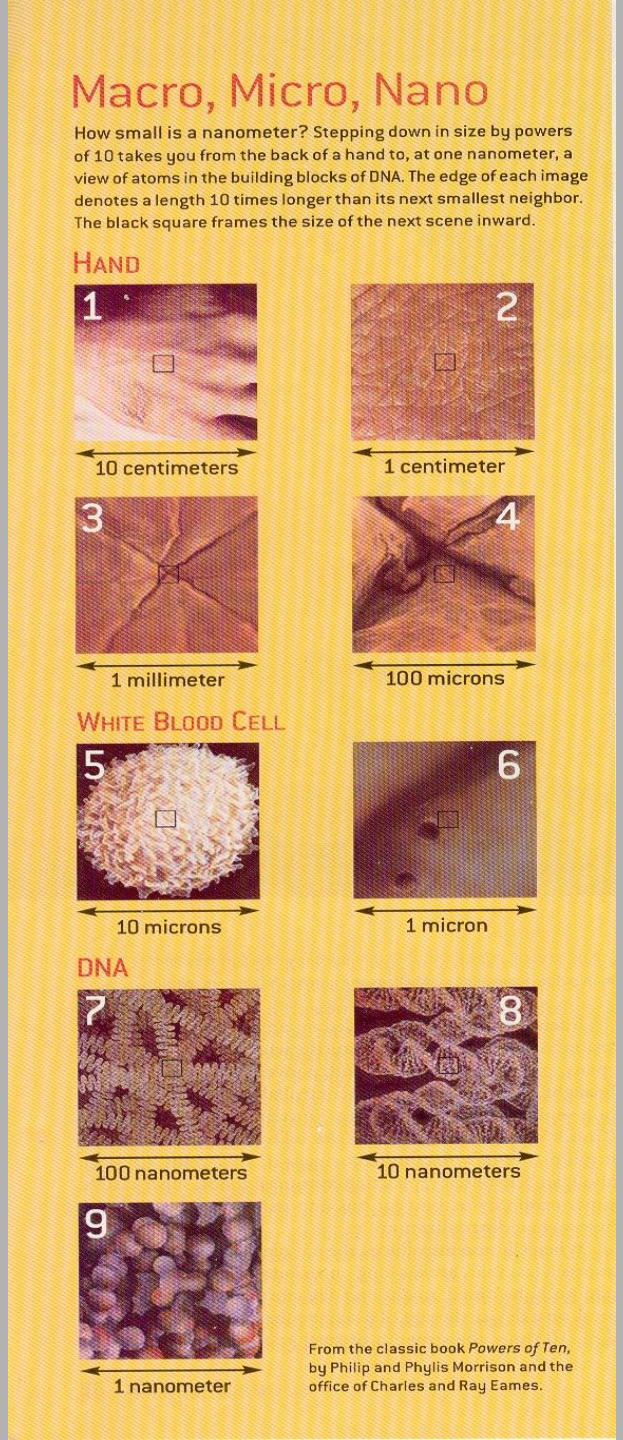

Periodická tabulka: struktura elektronového obalu dána protonovým číslem

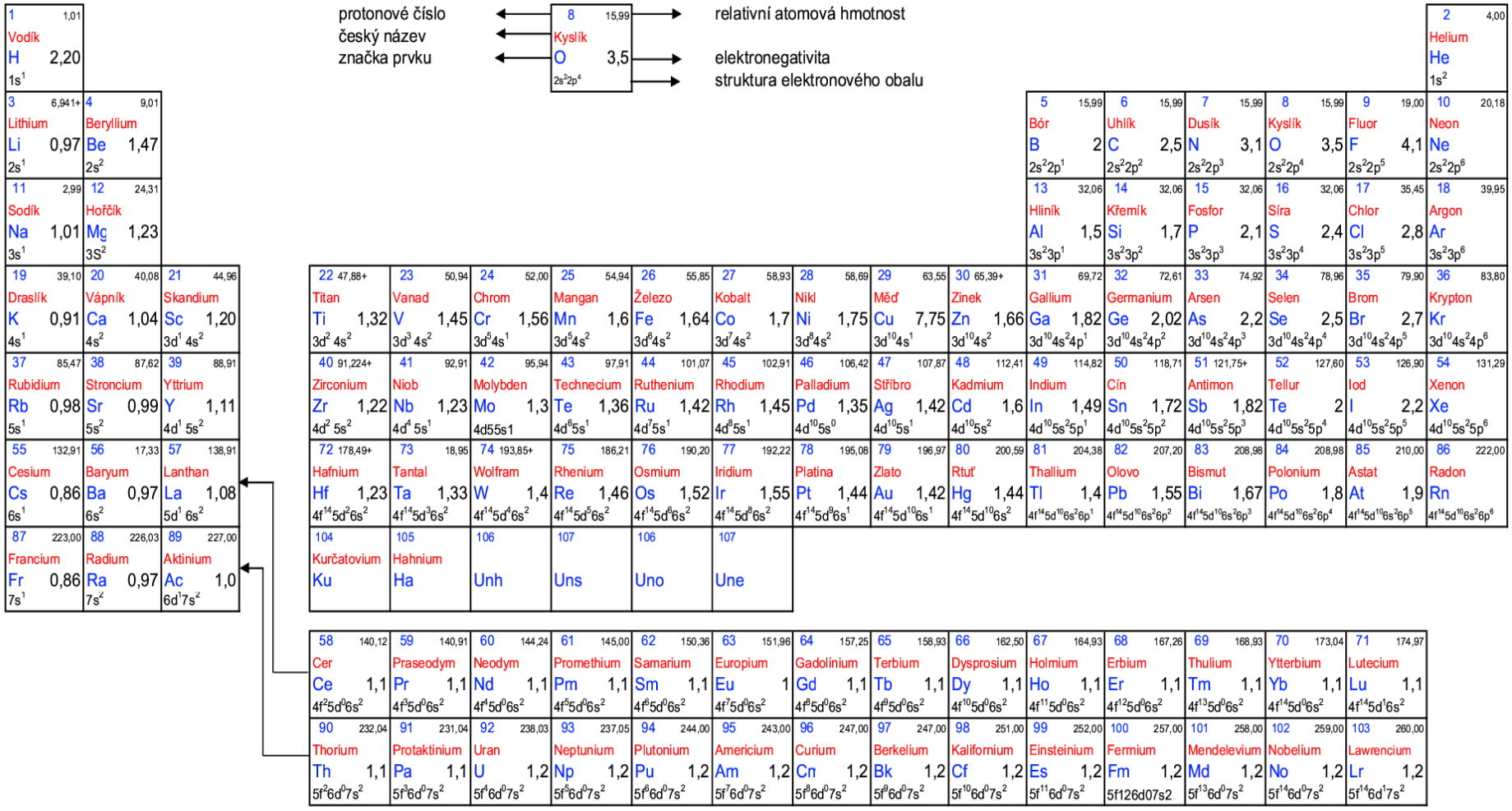

STM – „Scanning Tunneling Microscope“

Click on banner to return to Nobel Prize Internet Archive homepage

GERD BINNIG and HEINRICH ROHRER

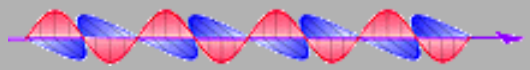

1986 Nobel Laureates in Physics

for their design of the scanning tunneling microscope.

Background

GERD BINNIG, 1947-1988
Residence: Federal Republic of Germany
Affiliation: IBM Zürich Research Laboratory, Rüschlikon, Switzerland

HEINRICH ROHRER, born: 1933
Residence: Switzerland
Affiliation: IBM Zürich Research Laboratory, Rüschlikon, Switzerland

STM – „Scanning Tunneling Microscope“

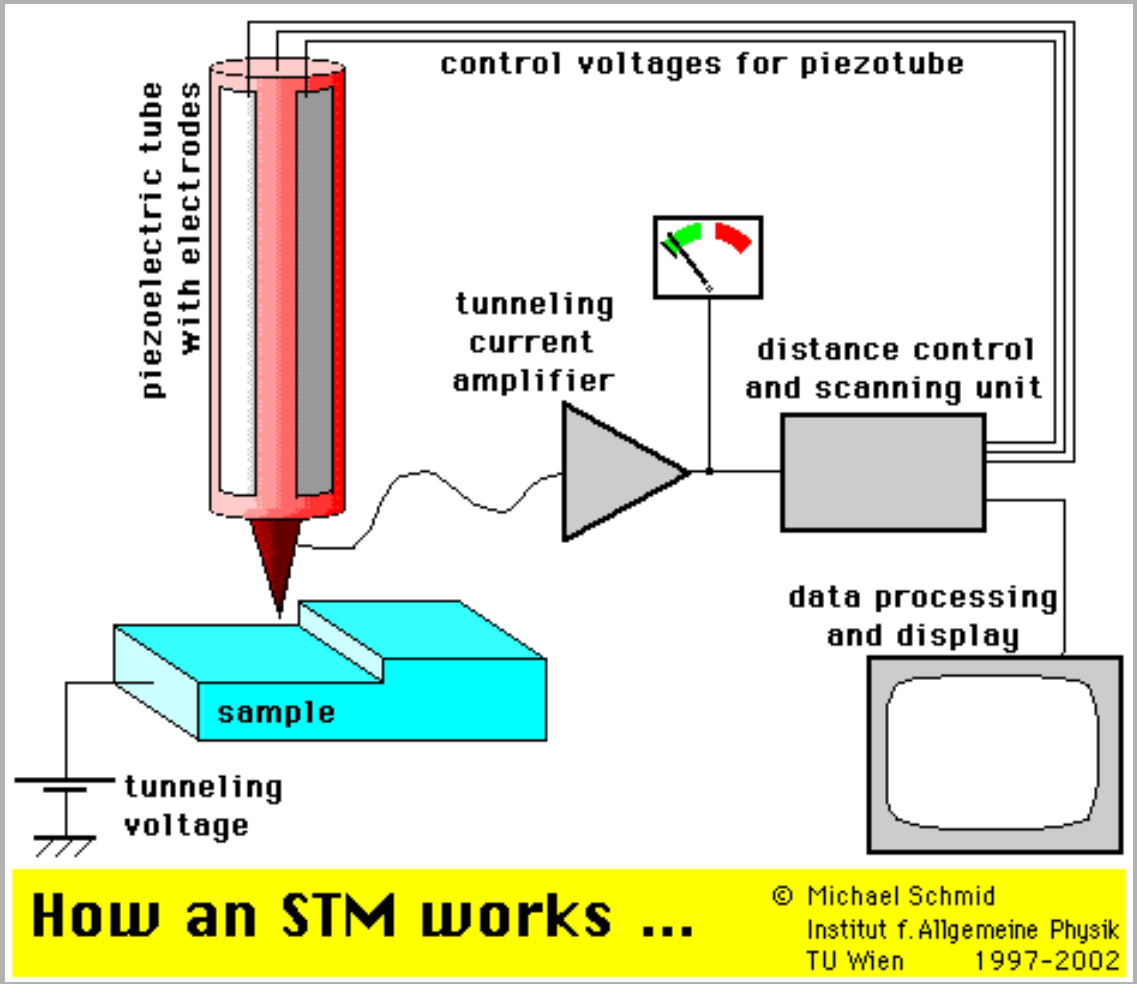

STM: povrchová rekonstrukce PtNi (černě: segregovaný C)

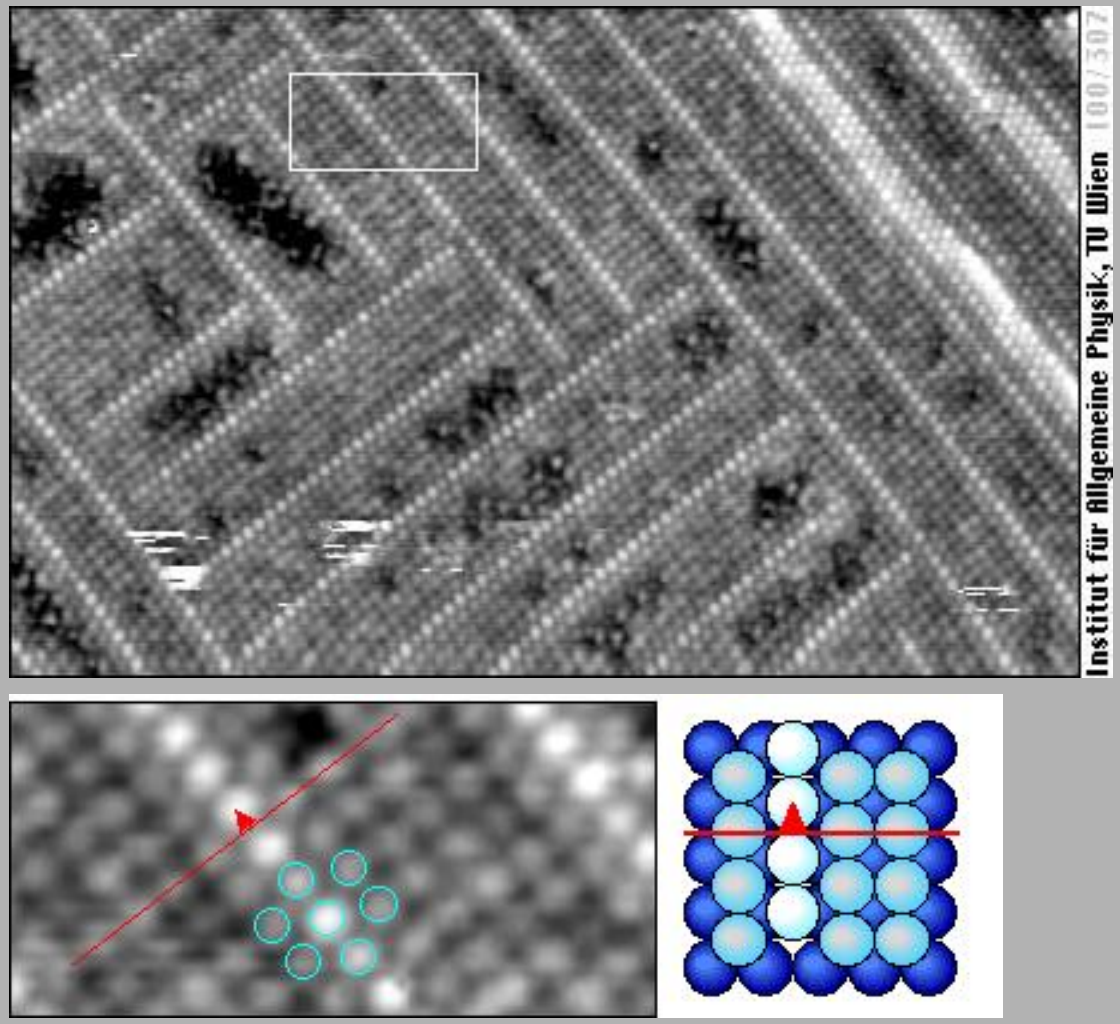

AFM – „Atomic Force Microscope“

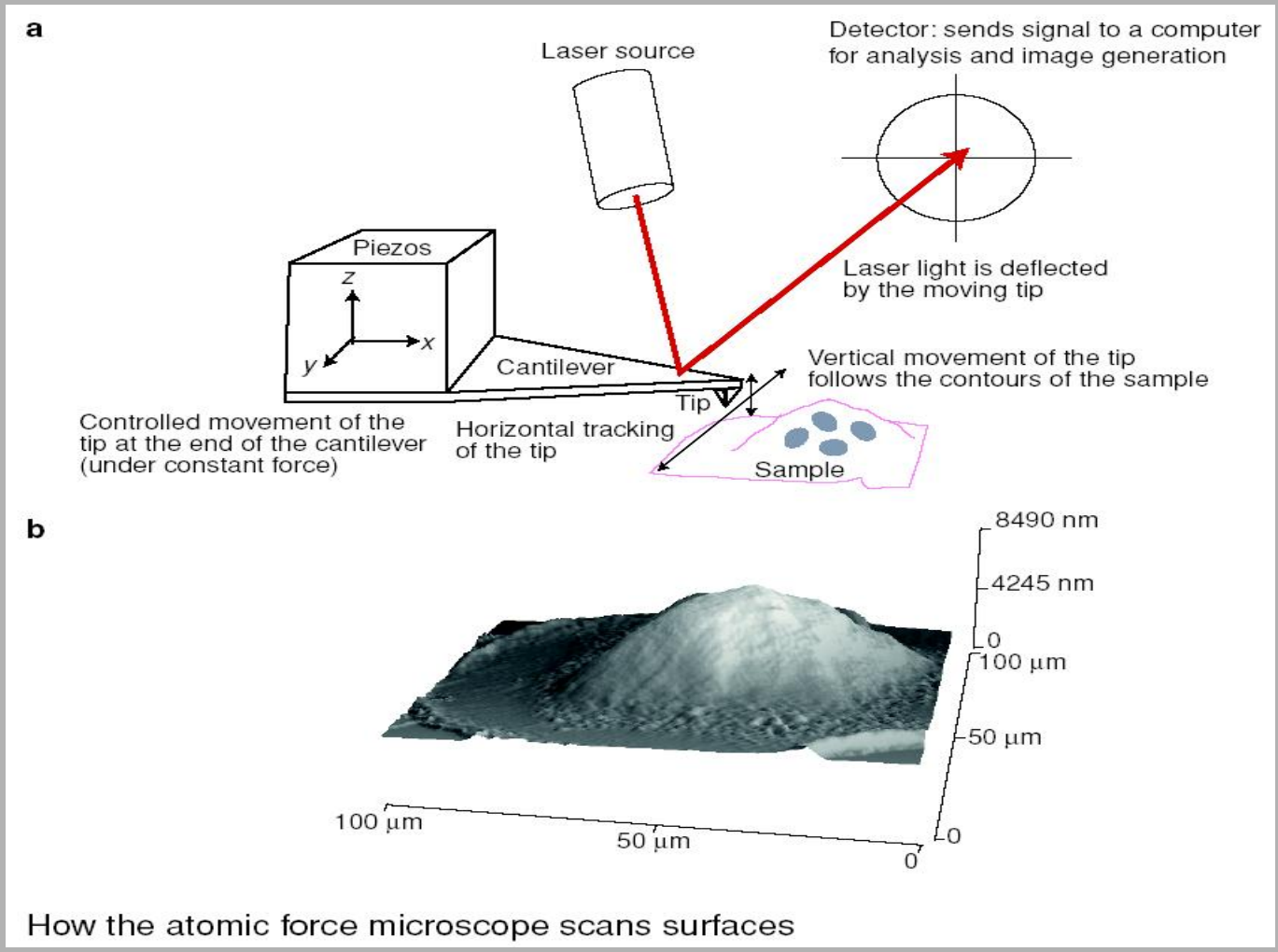

How the atomic force microscope scans surfaces

SPM

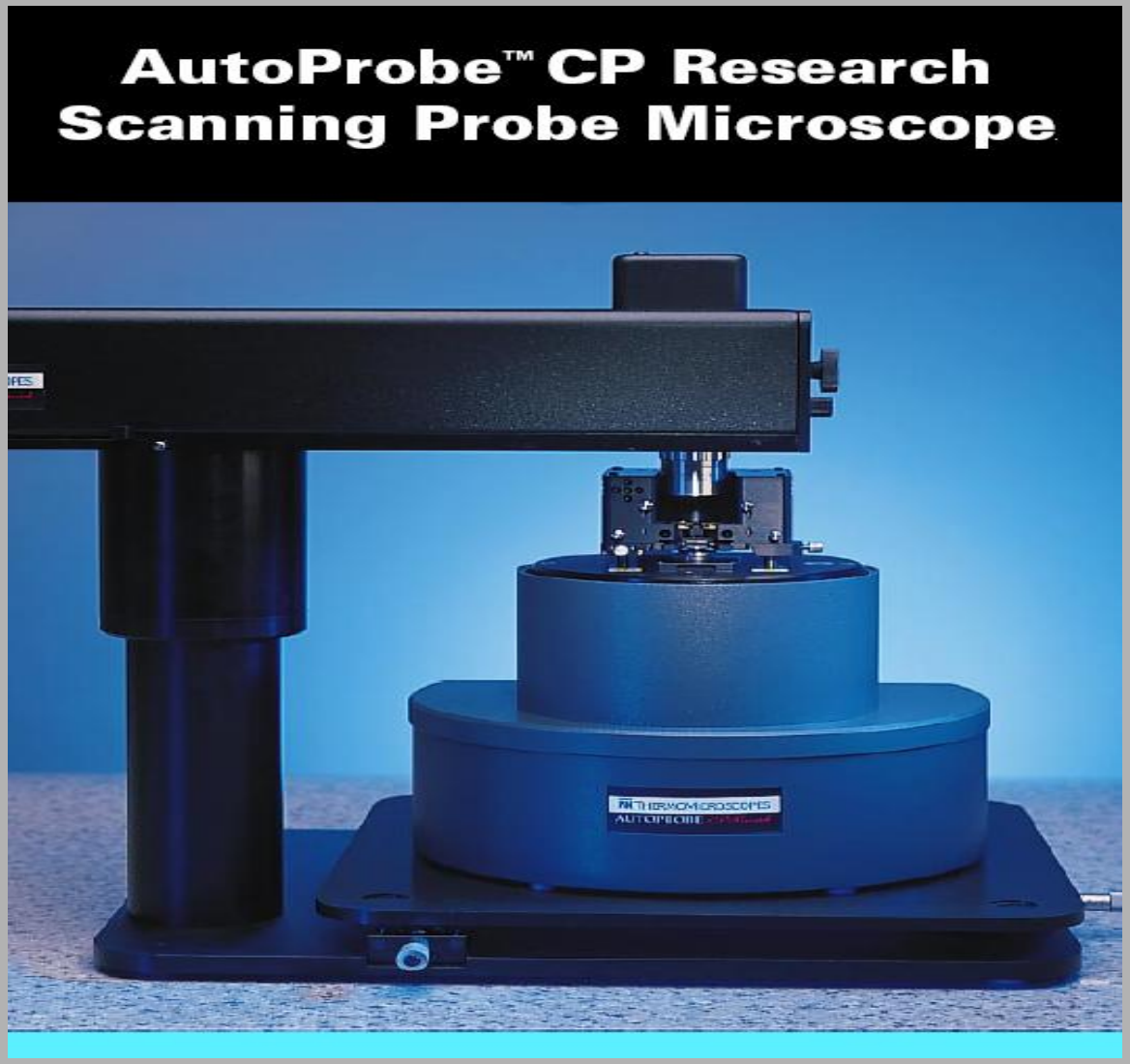

AFM: 671C (3xInAs/GaAs QD)

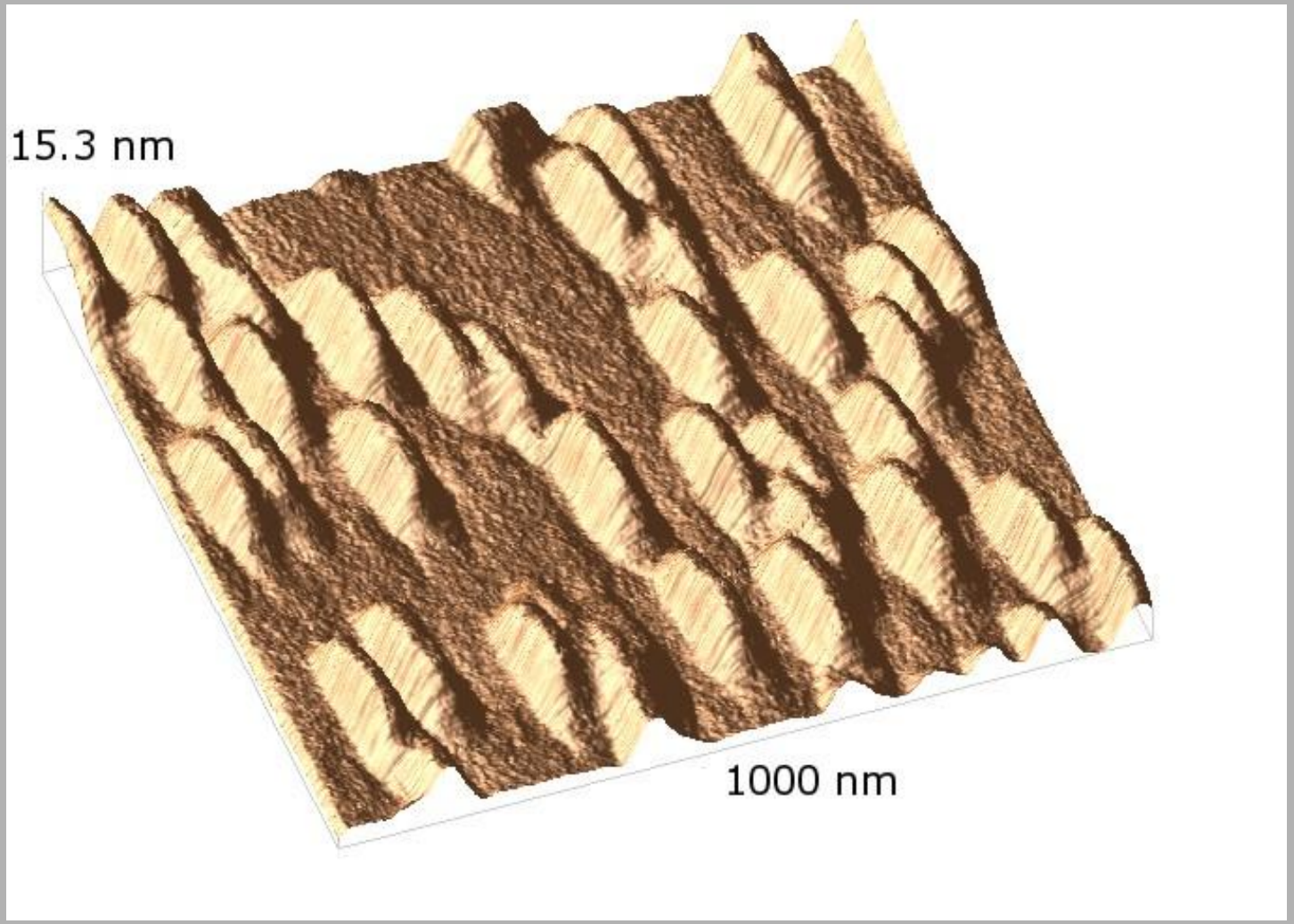

MBE SiGe/Si

(a)

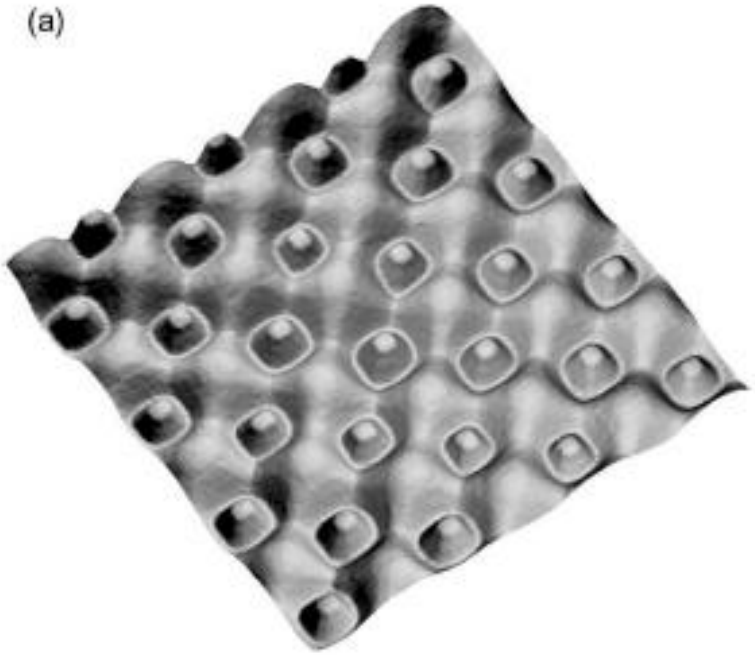

(b)

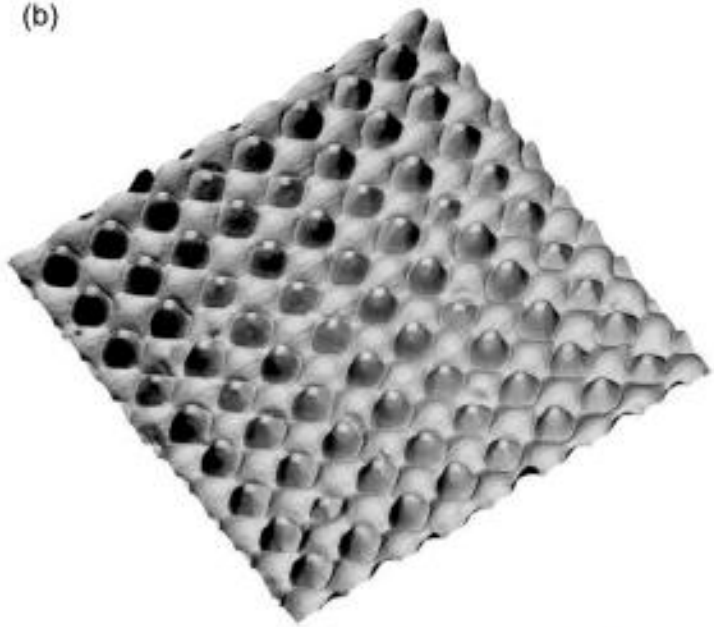

FIG. 1. Atomic force micrographs of the samples (a) *S*1 (pit period 300 nm) and (b) *S*2 (pit period 170 nm). The scanned area was 1.5 × 1.5 μm for both samples. The average height of the QDs in sample *S*1 (*S*2) is 15.3 (15) nm and the QD base diameter is 122.8 (118) nm.

Manipulace:

IBM Almaden

D.M. Eigler and E.K. Schweizer,

Positioning single atoms with a scanning tunneling microscope,

Nature 344, 524 (1990)

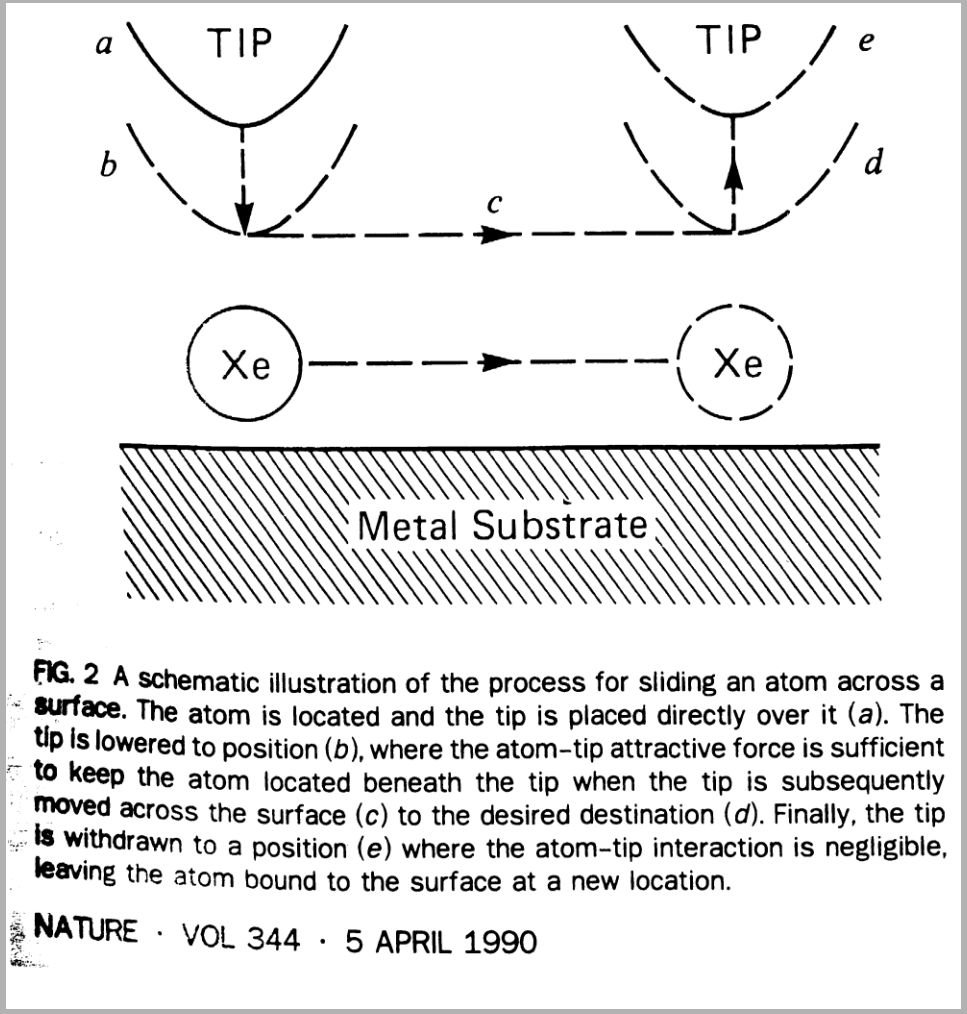

FIG. 2 A schematic illustration of the process for sliding an atom across a surface. The atom is located and the tip is placed directly over it (*a*). The tip is lowered to position (*b*), where the atom–tip attractive force is sufficient to keep the atom located beneath the tip when the tip is subsequently moved across the surface (*c*) to the desired destination (*d*). Finally, the tip is withdrawn to a position (*e*) where the atom–tip interaction is negligible, leaving the atom bound to the surface at a new location.

NATURE · VOL 344 · 5 APRIL 1990

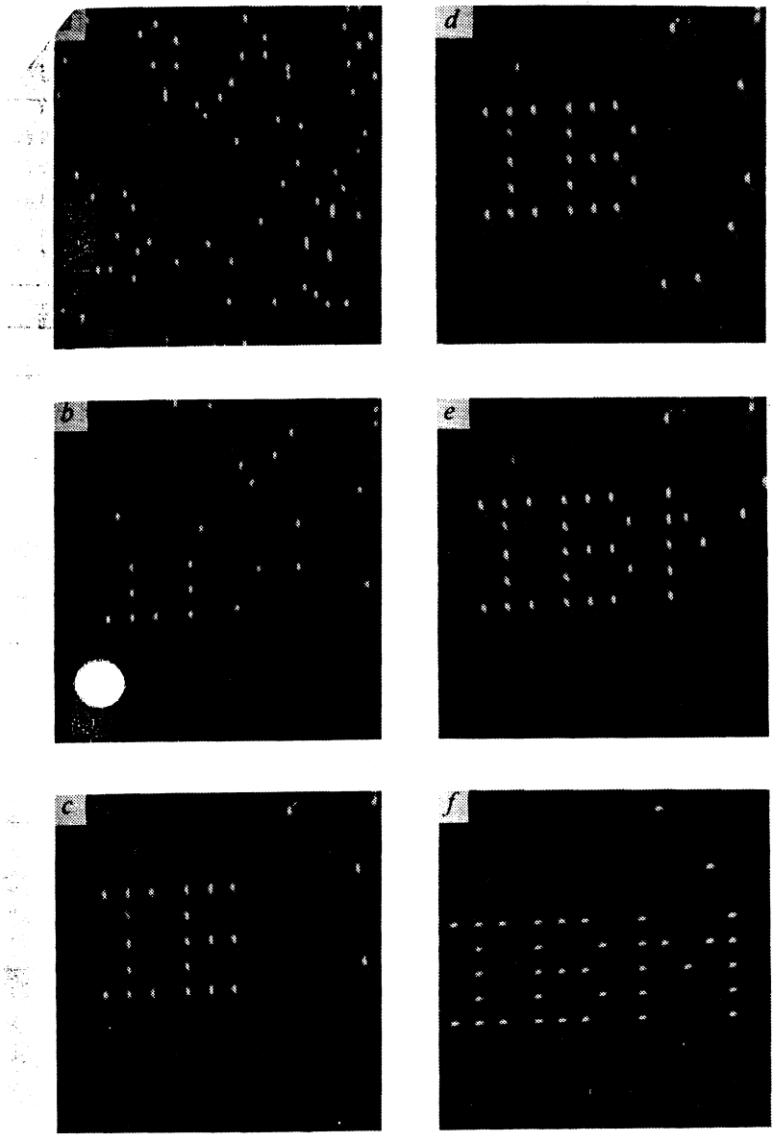

FIG. 1. A sequence of STM images taken during the construction of a patterned array of xenon atoms on a nickel (110) surface. Grey scale is assigned according to the slope of the surface. The atomic structure of the nickel surface is not resolved. The $\langle 1\bar{1}0 \rangle$ direction runs vertically. *a*, The surface after xenon dosing. *b*–*f*, Various stages during the construction. Each letter is 50 Å from top to bottom.

STM: 4K, Cu(111) + 48 atomů Fe, průměr kroužku 14.3 nm
Crommie et. at., IBM Almaden Research Center

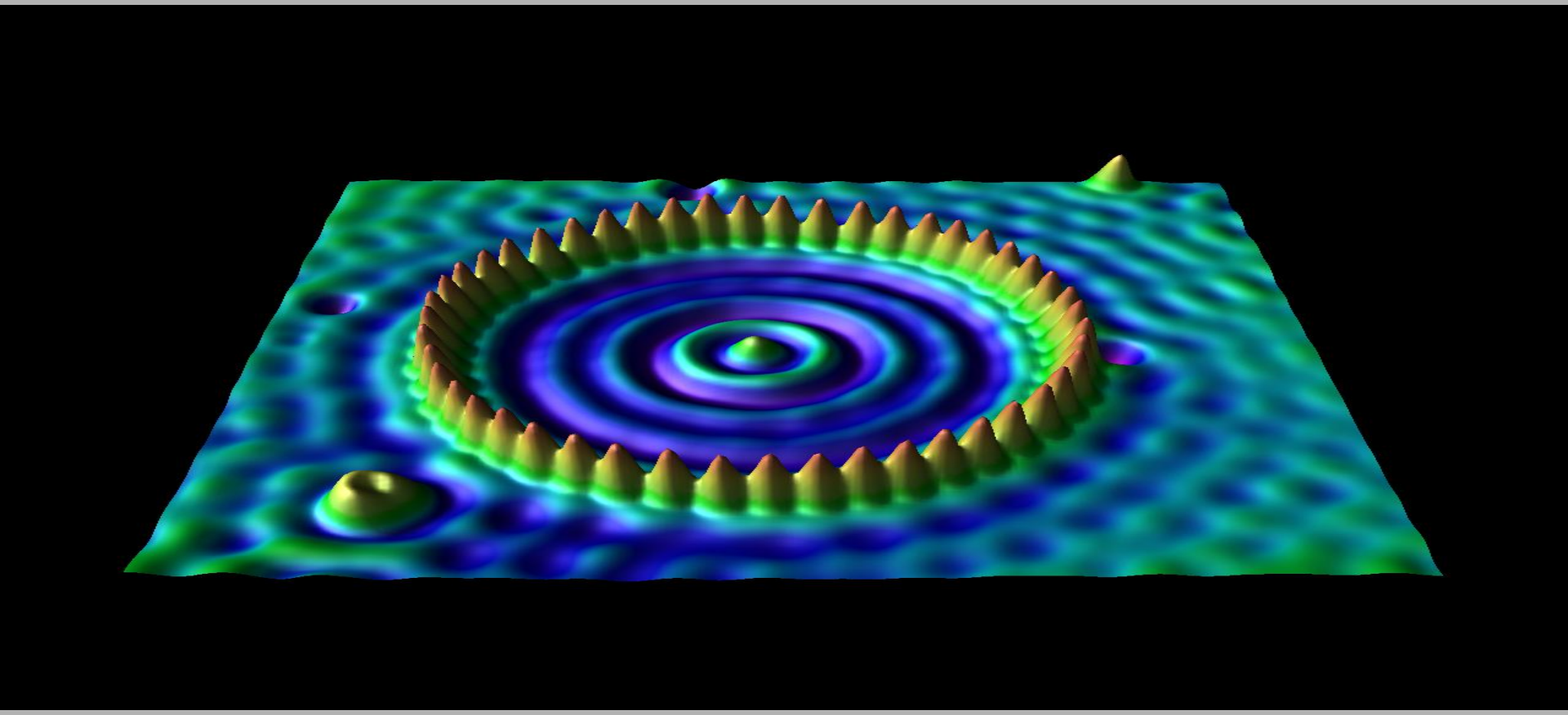

InAs/InP Quantum Wires (L. Samuelson, Univ. Lund)

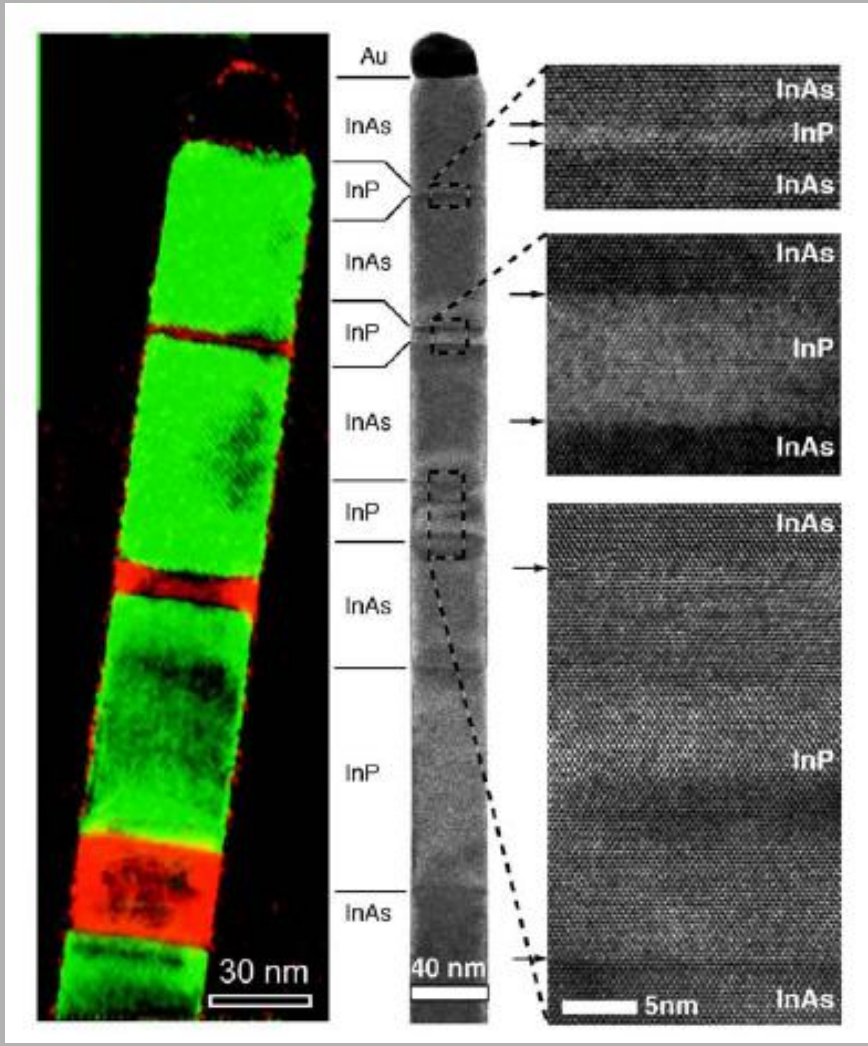

Fig. 1. Left-hand figure shows a color-coded representation of the origin of diffraction spots from the two lattices of InAs (green) and InP (red). The right-hand figure shows a high-resolution electron microscope image of the same structure from which one can deduce that the multiple layer structure of alternating InAs and InP segments are perfect from a crystalline point of view, are free of strain within less than 10 nm from the interface, and have an interface abruptness on the atomic level.

GaAs Wires (L. Samuelson, Univ. Lund)

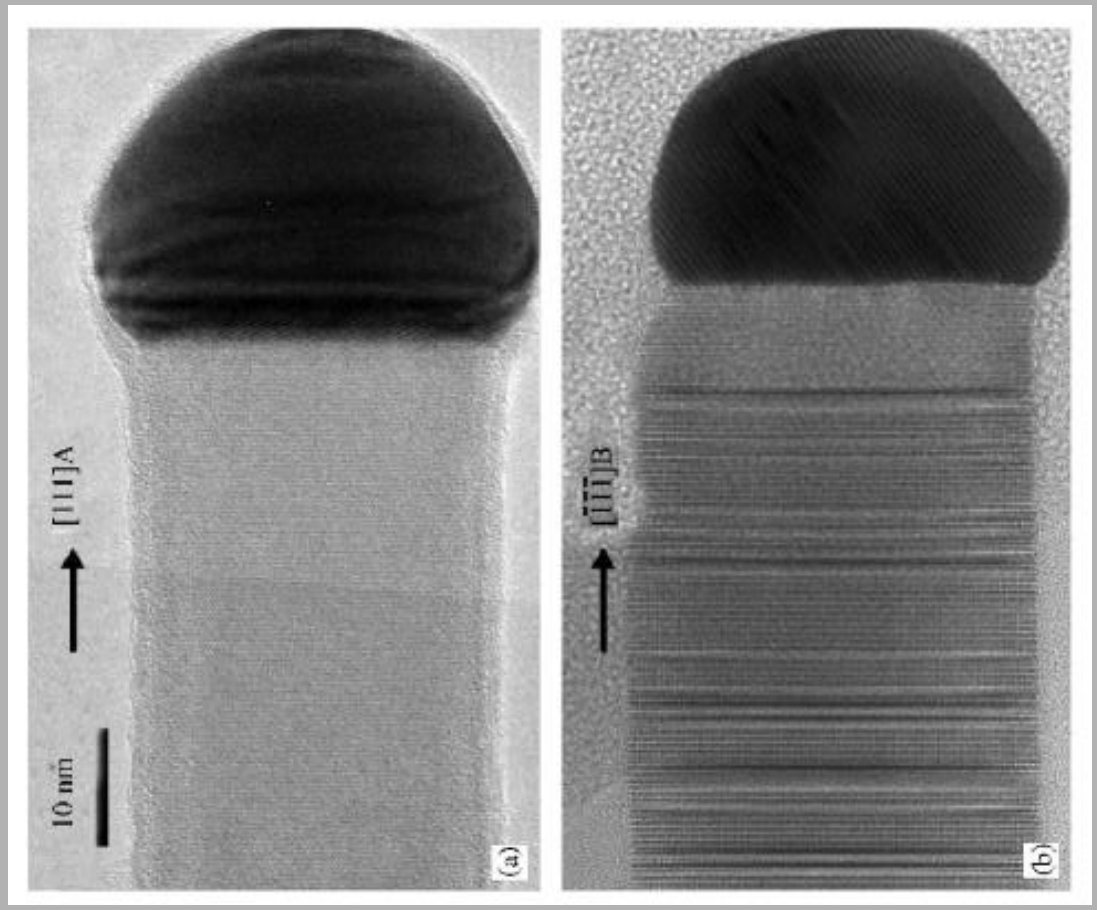

Fig. 3. TEM images of GaAs wires with a dark gold particle at the end of each wire. 10 nm scale bar. (a) Stacking fault free wire grown in the [1 1 1]*A* direction. (b) [$\bar{1}\ \bar{1}\ \bar{1}$]*B* wire with stacking faults as evidenced by the dark lines perpendicular to the growth direction.

GaP nanotrees (L. Samuelson, Univ. Lund)

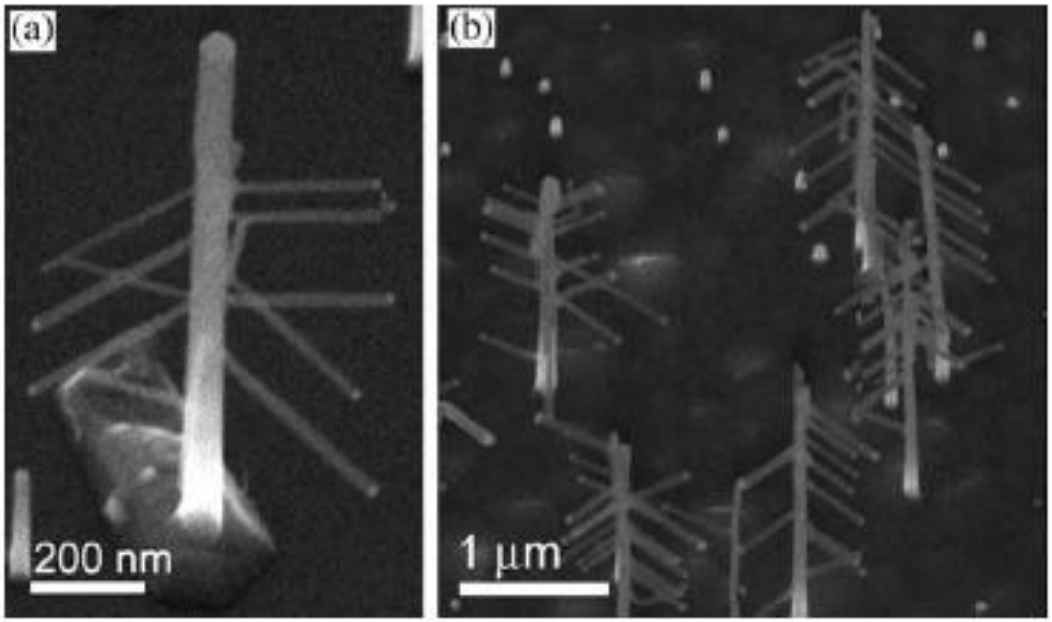

Fig. 1. SEM images of branched GaP nanotrees: (a) Single nanotree, tilt 45° from normal to the surface. This sample was grown at 460 °C, 1.25×10^{-5} molar fraction TMG, 7.5×10^{-3} molar fraction PH_3, trunk growth time 4 min, branch growth time 90 s. (b) Nano-"forest" shown tilted 30° from normal to the surface, growth conditions as above, except branch growth time 60 s.

InAs/InP Quantum Wires (L. Samuelson, Univ. Lund)

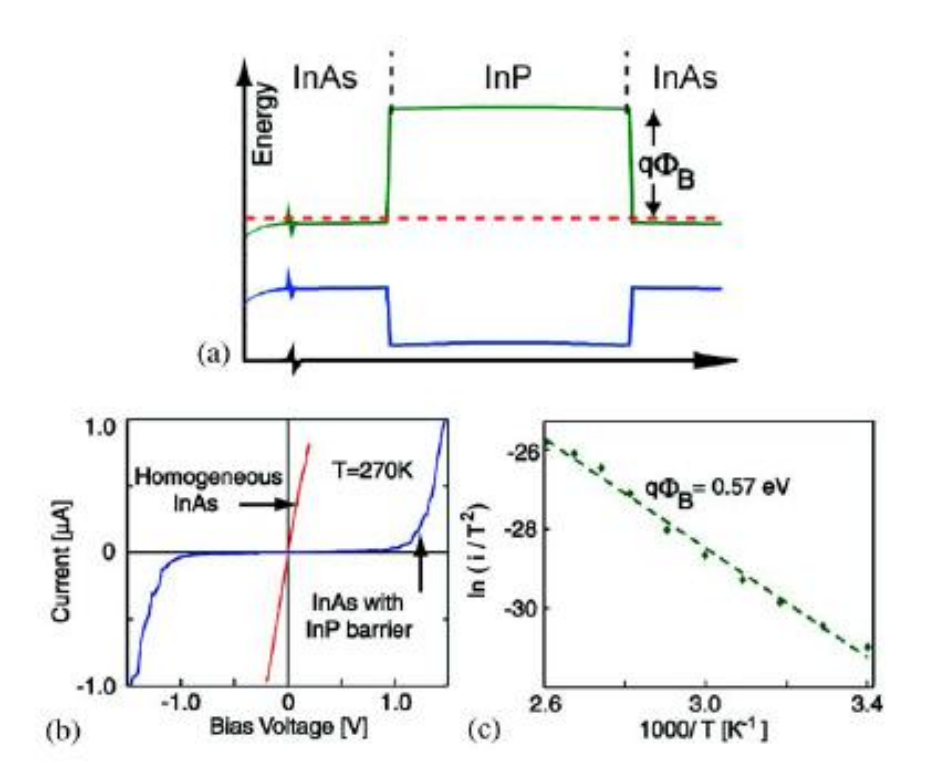

Fig. 2. (a) Band diagram of a single barrier nanowire. (b) A comparison between the I–V characteristics of a homogeneous n-type InAs nanowire and one with an 80 nm thick InP barrier inserted. Thermal activation of the current, (c), gives an activation energy of about 0.6 eV for the conduction band offset.

Kvantové tečky InAs/GaAs (MOVPE FzÚ AV ČR Praha, ÚFKL PřF MU Brno)

TEM: 7 vstev, spacer 7.5 nm, vertikální korelace

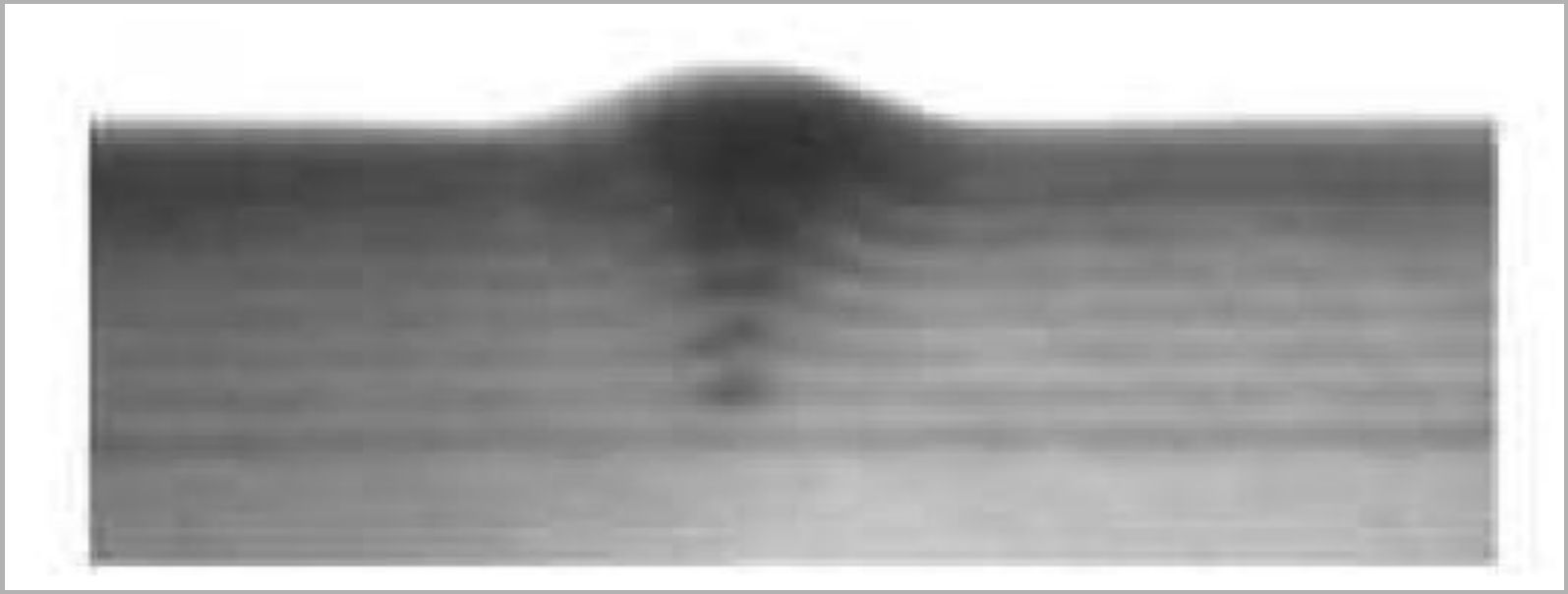

Kvantové tečky InAs/GaAs (ÚFKL PřF MU Brno)

„confining potential“, osa tečky

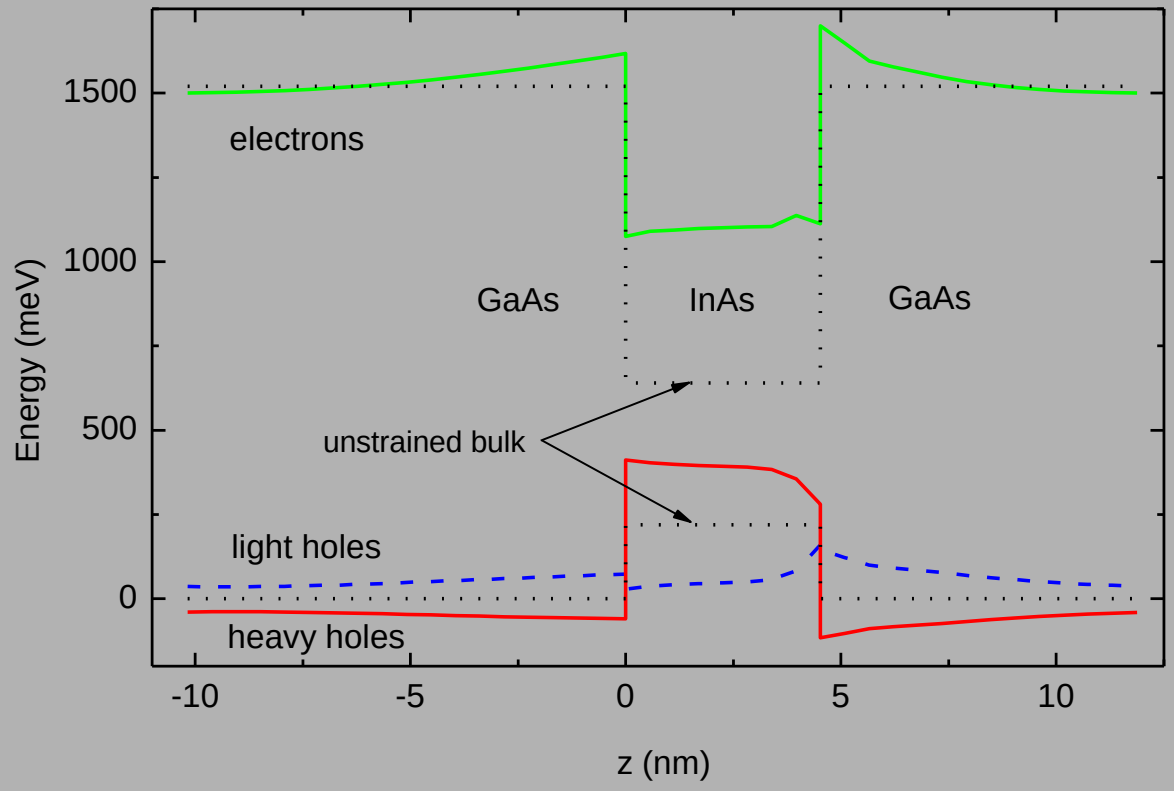

Kvantové tečky InAs/GaAs
(ÚFKL PřF MU Brno)

„confining potential“
v ploše

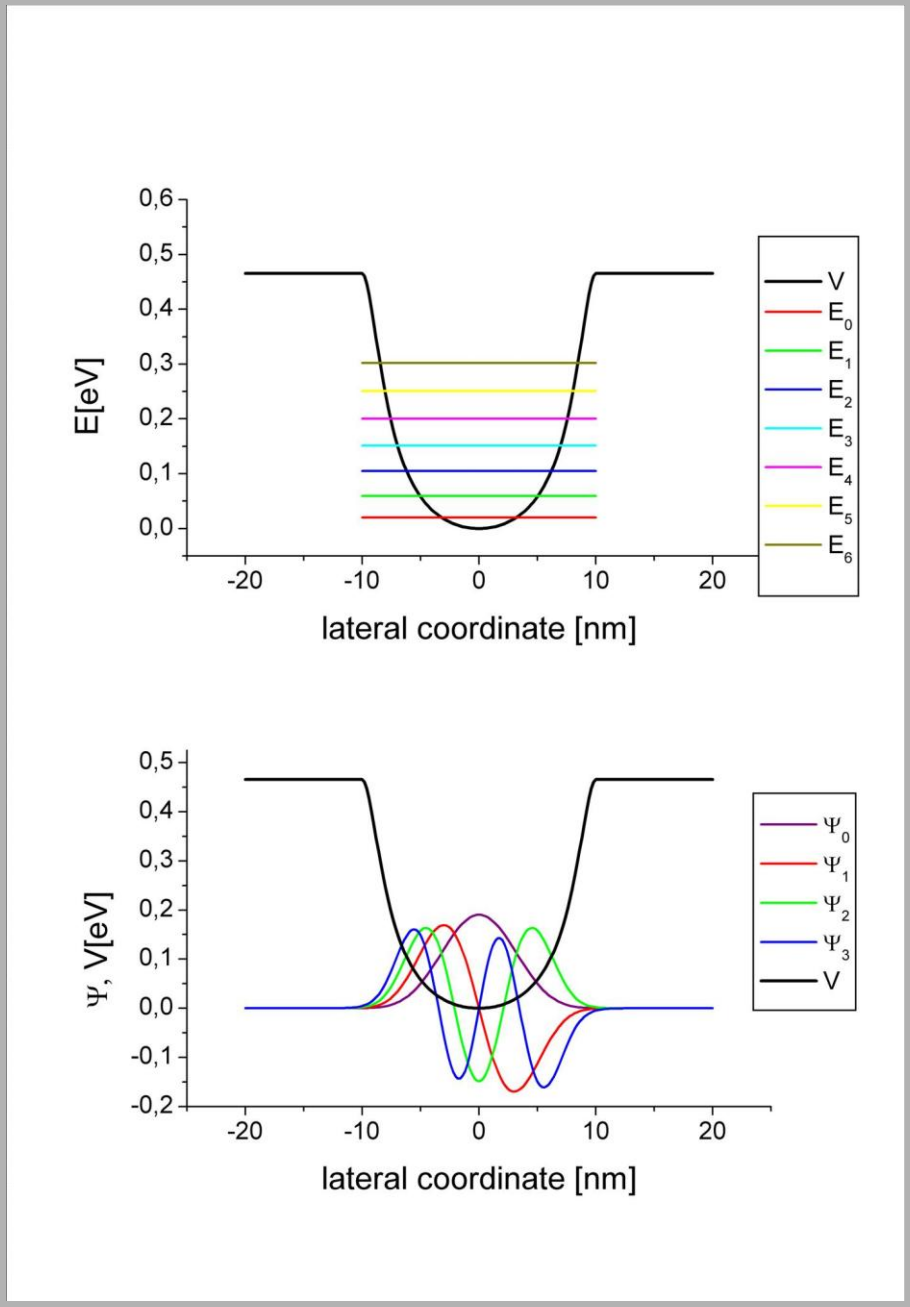

Kvantové tečky InAs/GaAs

snaha o dosažení emise s vlnovou délkou 1.3 a 1.55 μm

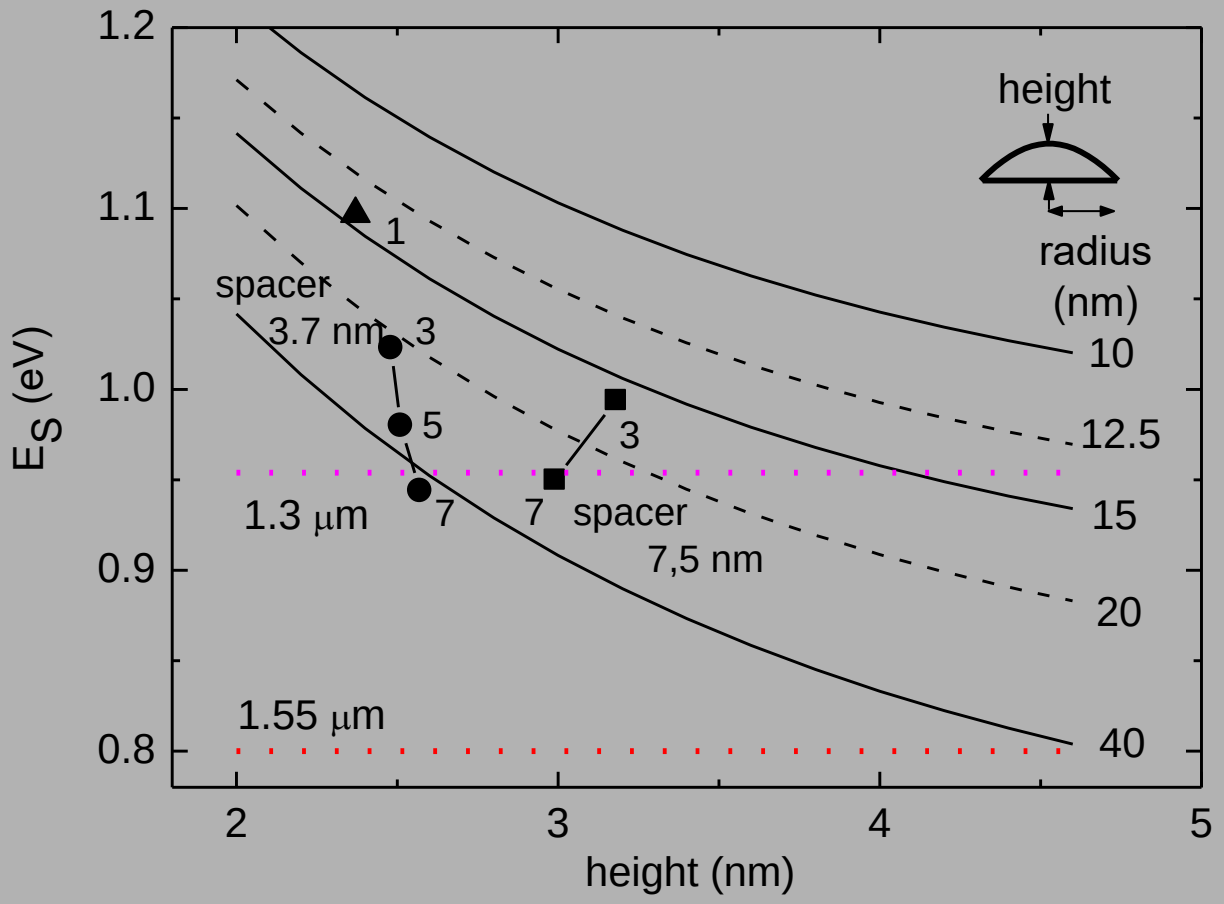

Známý (slabý) vliv magnetického pole na vedení proudu

Lord Kelvin, 1856

W. Thomson, "On the Electro-Dynamic Qualities of Metals: Effects of Magnetization on the Electric Conductivity of Nickel and of Iron", Proceedings of the Royal Society of London, **8**, pp. 546–550 (1856–1857).

Překvapení roku 1988

„Gigantická magnetorezistence" (GMR) v kovových multivrstvách

G. Binasch, P. Grünberg, F. Saurenbach, and W. Zinn, "Enhanced magnetoresistance in layered magnetic structures with antiferromagnetic interlayer exchange", Phys. Rev. B **39**, 4828 (1989).

M.N. Baibich, J.M. Broto, A. Fert, F. Nguyen van Dau, F. Petroff, P. Eitenne, G. Creuzet, A. Friederich, and J. Chazelas, "Giant Magnetoresistance of (001)Fe/(001)Cr Magnetic Superlattices", Phys. Rev. Lett. **61**, 2472 (1988).

Překvapení roku 1988

„Gigantická magnetorezistence“ (GMR) v kovových multivrstvách

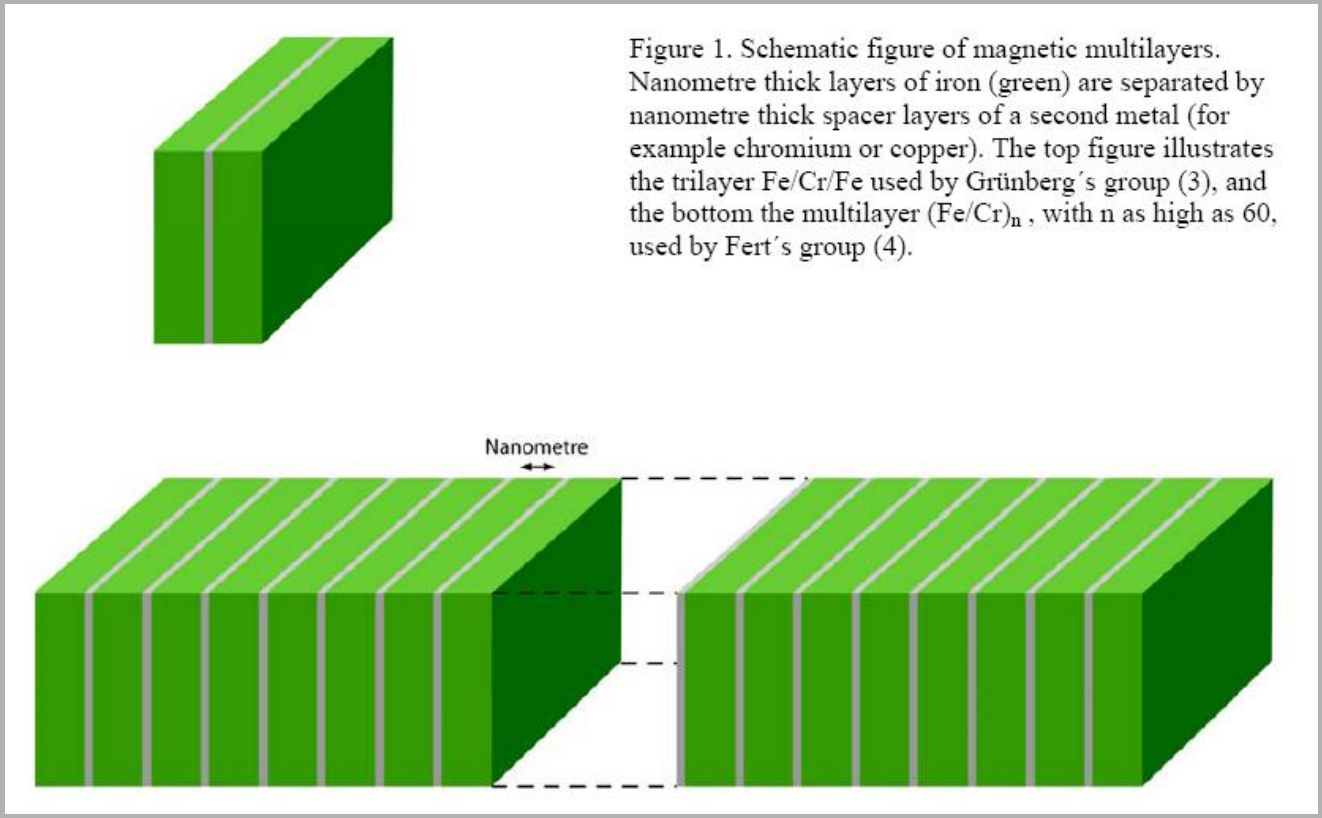

Figure 1. Schematic figure of magnetic multilayers. Nanometre thick layers of iron (green) are separated by nanometre thick spacer layers of a second metal (for example chromium or copper). The top figure illustrates the trilayer Fe/Cr/Fe used by Grünberg´s group (3), and the bottom the multilayer $(Fe/Cr)_n$, with n as high as 60, used by Fert´s group (4).

P. Gruenberg (Juelich): Fe/Cr/Fe

A. Fert (Paris Sud): $(Fe/Cr)_n$ n ~ 60

Překvapení roku 1988

„Gigantická magnetorezistence“ (GMR) v kovových multivrstvách

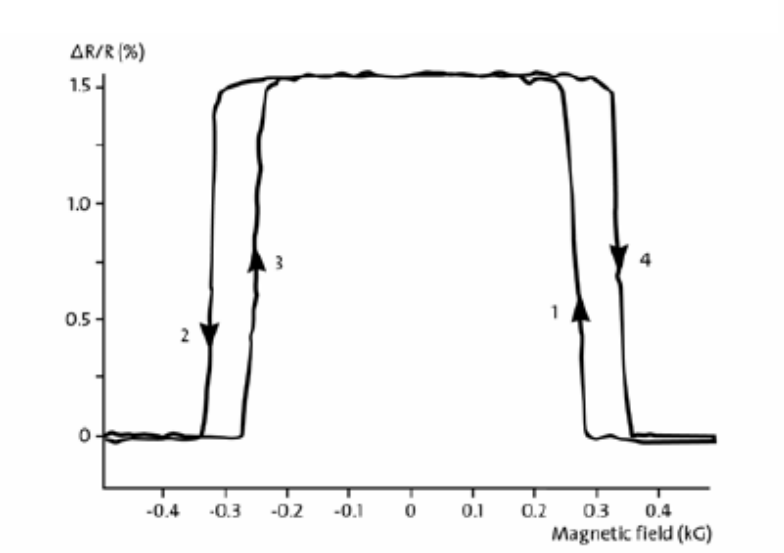

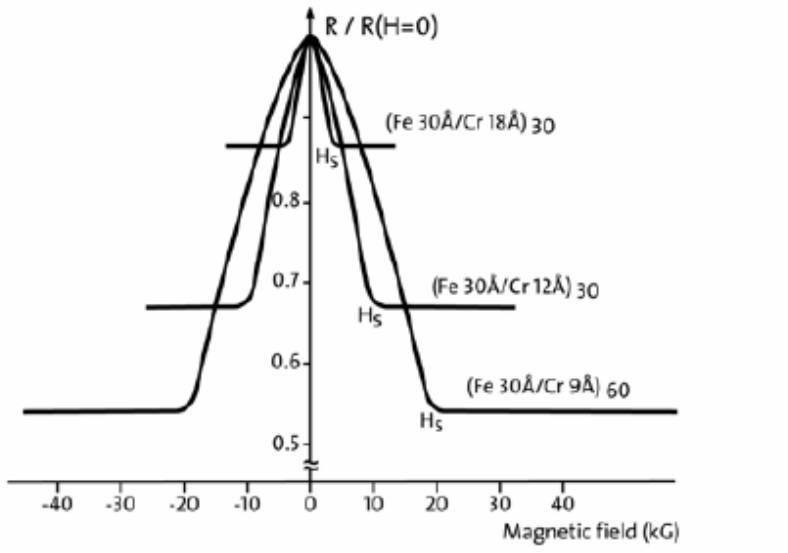

Figure 2. After refs. (3) and (4).
Left: Magnetoresistance measurements (3) (room temperature) for the trilayer system Fe/Cr/Fe. To the far right as well as to the far left the magnetizations of the two iron layers are both parallel to the external magnetic field. In the intermediate region the magnetizations of the two iron layers are antiparallel. The experiments also show a hysterisis behaviour (difference 1 and 4 (2 and 3)) typical for magnetization measurements.
Right: Magnetoresistance measurements (4) (4.2K) for the multilayer system $(Fe/Cr)_n$. To the far right ($>H_S$, where H_S is the saturation field) as well as to the far left ($< -H_S$) the magnetizations of all iron layers are parallel to the external magnetic field. In the low field region every second iron layer is magnetized antiparallel to the external magnetic field. 10 kG = 1 Tesla.

Spinová polarizace v přechodových kovech

nemagnetický magnetický

stav

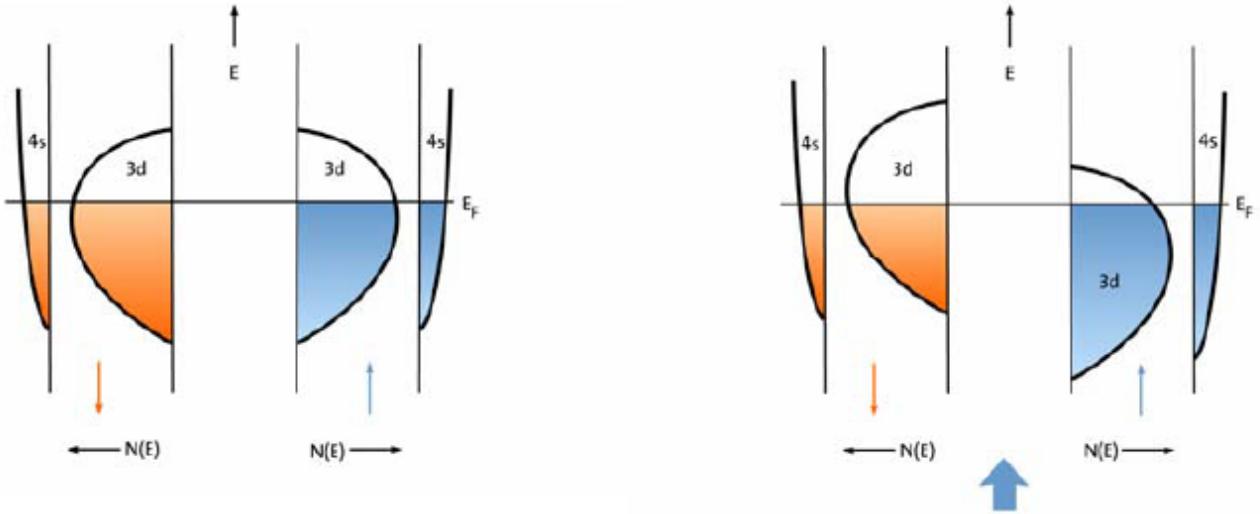

Figure 3. **To the left** a schematic plot is shown for the energy band structure of a d transition metal. The density of states N(E) is shown separately for the spin up and down electrons and where a simplified separation has been made between the 4s and 3d band energies. For the non-magnetic state these are identical for the two spins. All energy levels below the Fermi energy are occupied states (orange and blue). The coloured area (orange + blue) corresponds to the total number of valence electrons in the metal. **To the right** the corresponding picture is illustrated for a ferromagnetic state, with a spin-polarization chosen to be in the up direction ($N_\uparrow > N_\downarrow$; blue area > orange area). This polarization is indicated by the thick blue arrow at the bottom figure to the right.

Nanotechnologie – růst kovových supermřížek

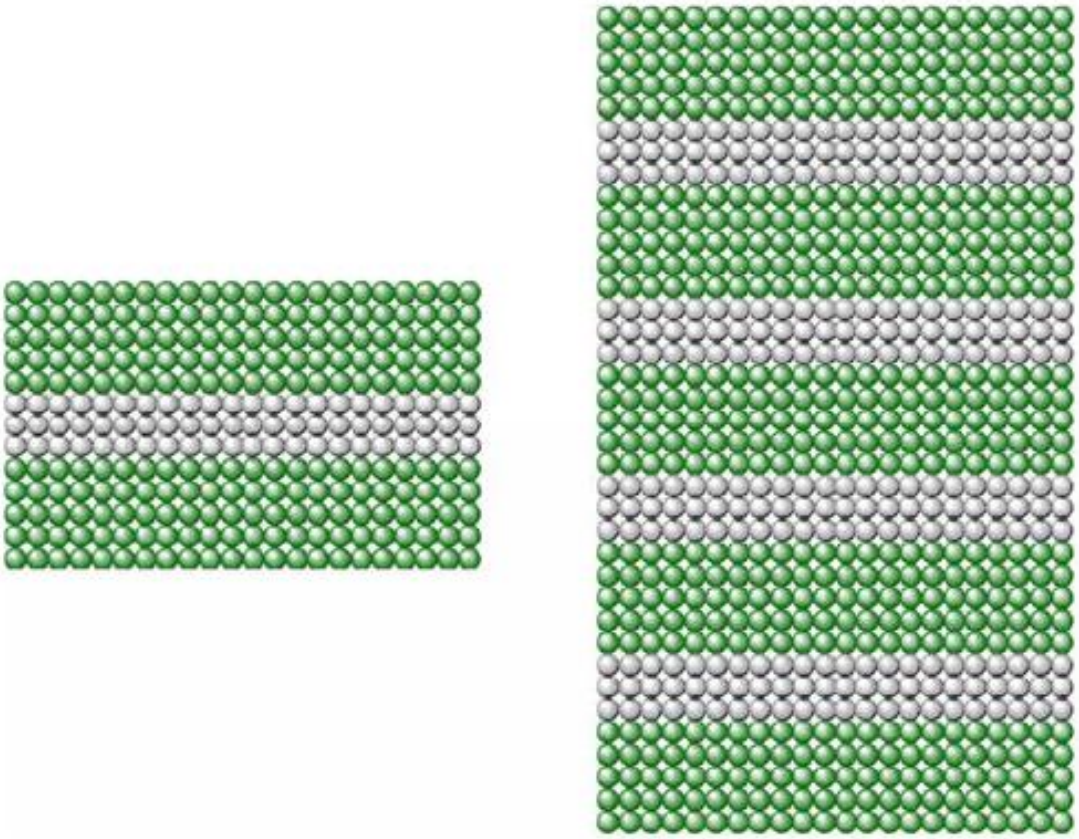

Figure 4. Illustration of superlattices. This is essentially the same figure as in figure 1, but now with atomic resolution. From this it becomes obvious that the lattice mismatch between the two materials needs to be small in order to be able to grow multilayers with well behaved interfaces.

Nemagnetická vrstva – vazba mezi magnetickými vrstvami

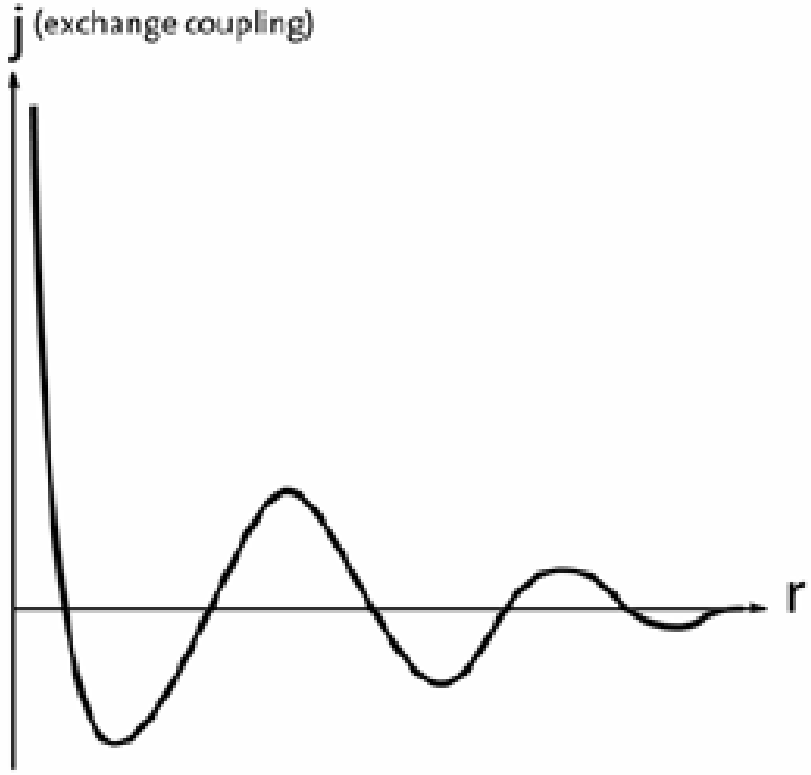

Figure 5. Schematic illustration of the behaviour of the exchange coupling as a function of distance.

„Giant MagnetoResistance“ (GMR) –

zvětšení proudu v magnetickém poli (paralelní magnetizace v dolní části obrázku)

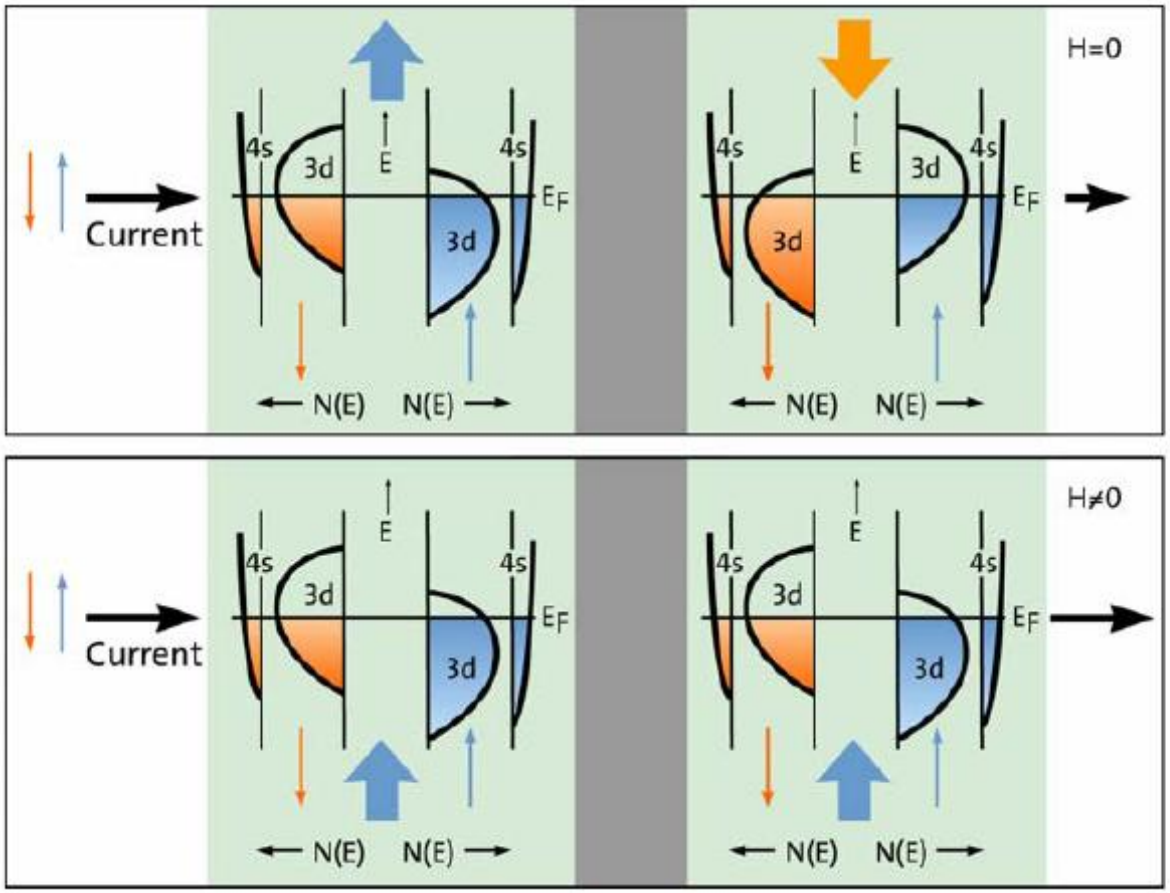

Figure 6. Schematic illustration of the electronic structure of a trilayer system with two ferromagnetic layers (light green) on both sides separated by nonmagnetic material (grey). The top figure is for the case without external magnetic field (H=0), i.e. when the two magnetic layers have opposite magnetizations (indicated by the thick blue and orange arrows at the top of the topmost figure). The bottom figure is for the case when an external magnetic field ($H \neq 0$) has forced the two magnetizations to be parallel (two thick blue arrows at the bottom of the lower figure.).The magnitude of the four magnetizations is the same.

„Náhradní schéma“ – různý příspěvek pohybu elektronů s opačnými spiny

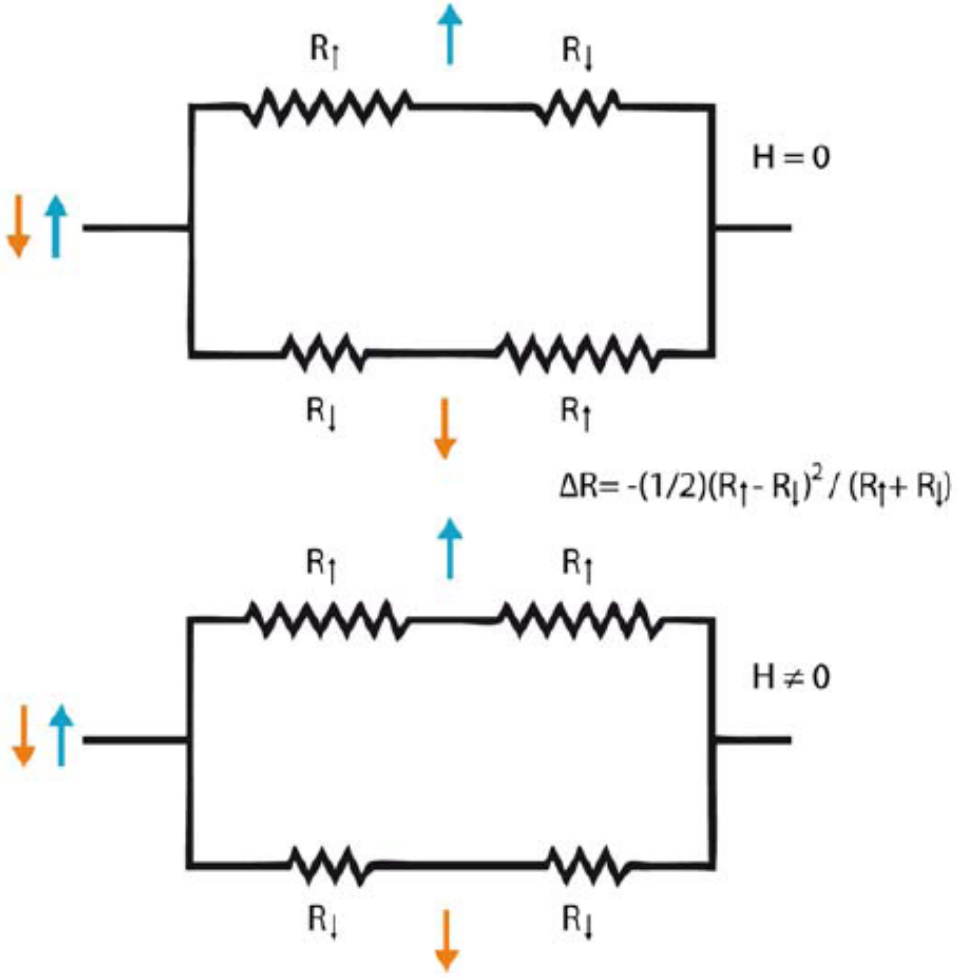

Figure 7. The same physical system as in figure 6. The magnetic layers are now represented by resistances $R_\uparrow$ and $R_\downarrow$. This shows very clearly that the total resistance for the two cases are different, i.e. there is a magnetoresistance effect. In case $R_\uparrow >> R_\downarrow$ it is practically only the lowest of the four possibilities which will permit a current. In the lower picture with parallel magnetizations the resistance for the spin up (spin down) electrons will be $R_\uparrow$ ($R_\downarrow$) in both magnetic layers. In the upper picture with antiparallel magnetizations the spin up (spin down) electrons will have a resistance $R_\uparrow$ ($R_\downarrow$) in the first magnetic layer to the left. In the second magnetic layer the resistance for the spin up (spin down) electron will be $R_\downarrow$ ($R_\uparrow$), since the magnetization environment has here become totally opposite compared to the first magnetic layer.

„TMR“ – magnetorezistivita ve struktuře s tunelovací vrstvou

Fe/MgO/Fe: $\Delta R/R \sim 0.5$ při pokojové teplotě

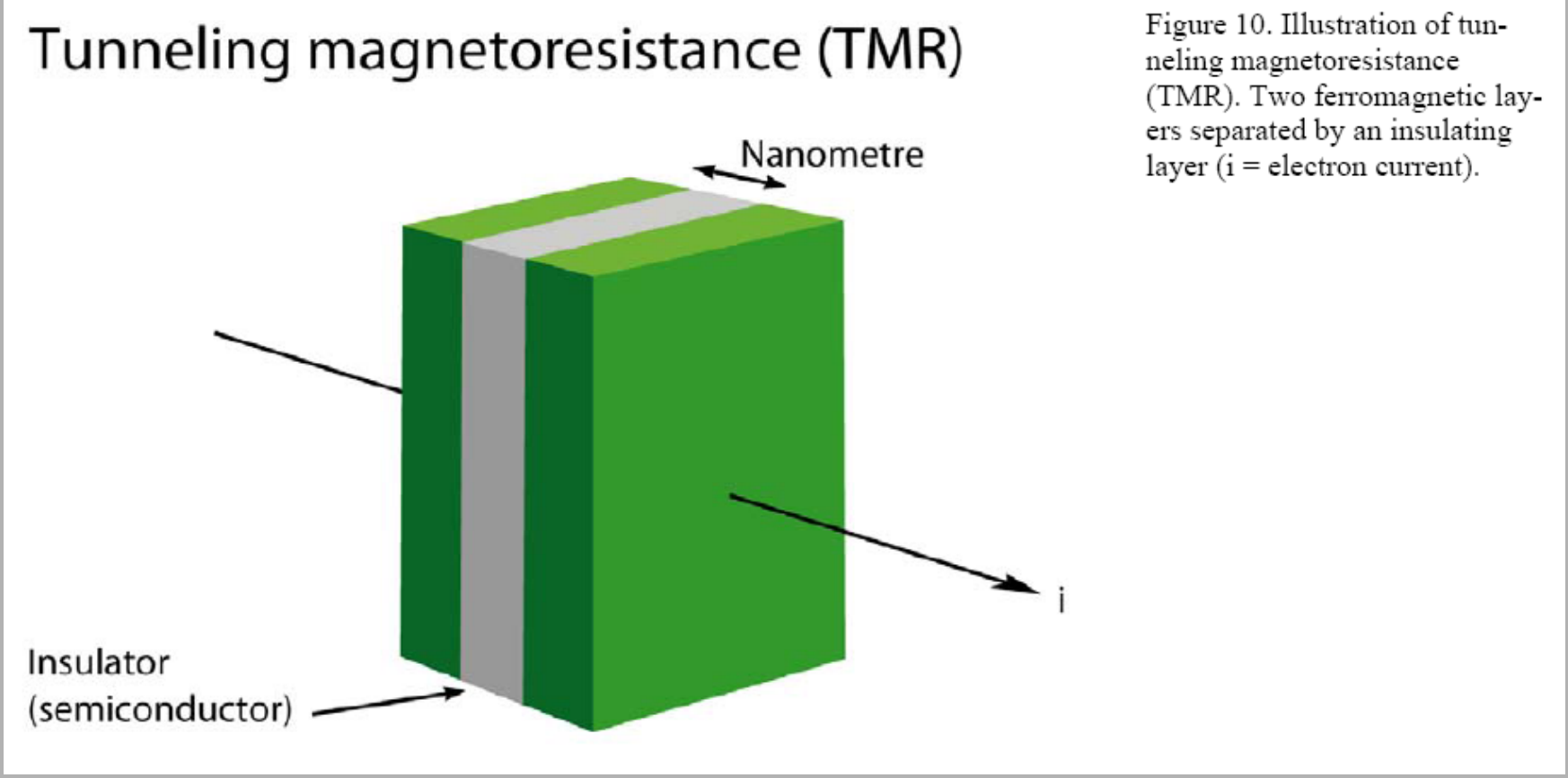

Figure 10. Illustration of tunneling magnetoresistance (TMR). Two ferromagnetic layers separated by an insulating layer (i = electron current).

Aplikace: magnetorezistivní hlavy v HD

Aplikace (?): magnetorezistivní paměť MRAM

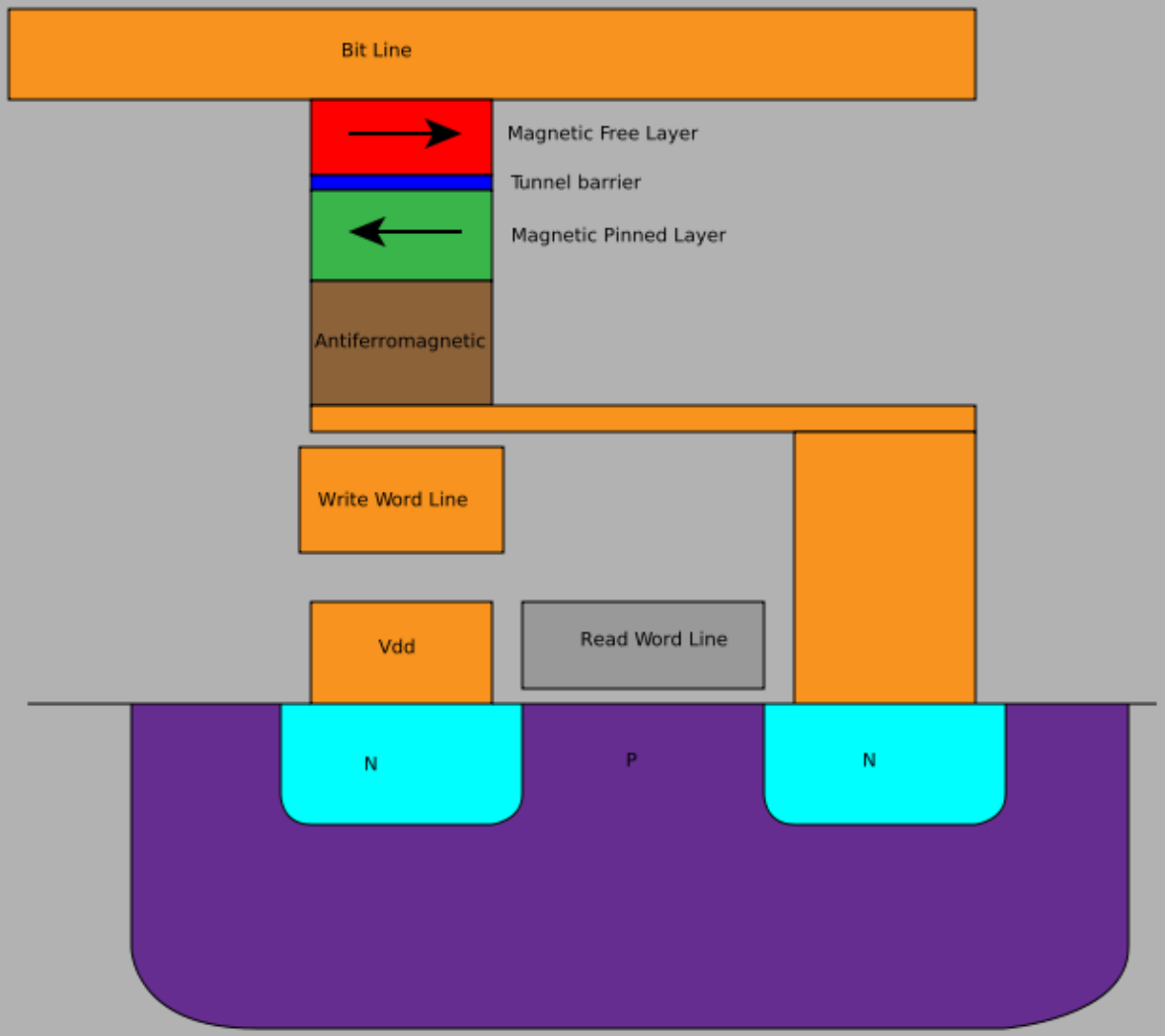

PRL 61, 2472 (1988):

VOLUME 61, NUMBER 21 PHYSICAL REVIEW LETTERS 21 NOVEMBER 1988

Giant Magnetoresistance of (001) Fe/(001) Cr Magnetic Superlattices

M. N. Baibich,[a] J. M. Broto, A. Fert, F. Nguyen Van Dau, and F. Petroff
Laboratoire de Physique des Solides, Université Paris-Sud, F-91405 Orsay, France

P. Eitenne, G. Creuzet, A. Friederich, and J. Chazelas
Laboratoire Central de Recherches, Thomson CSF, B.P. 10, F-91401 Orsay, France
(Received 24 August 1988)

We have studied the magnetoresistance of (001)Fe/(001)Cr superlattices prepared by molecular-beam epitaxy. A huge magnetoresistance is found in superlattices with thin Cr layers: For example, with $t_{Cr}=9$ Å, at $T=4.2$ K, the resistivity is lowered by almost a factor of 2 in a magnetic field of 2 T. We ascribe this giant magnetoresistance to spin-dependent transmission of the conduction electrons between Fe layers through Cr layers.

PRL 61, 2472 (1988):

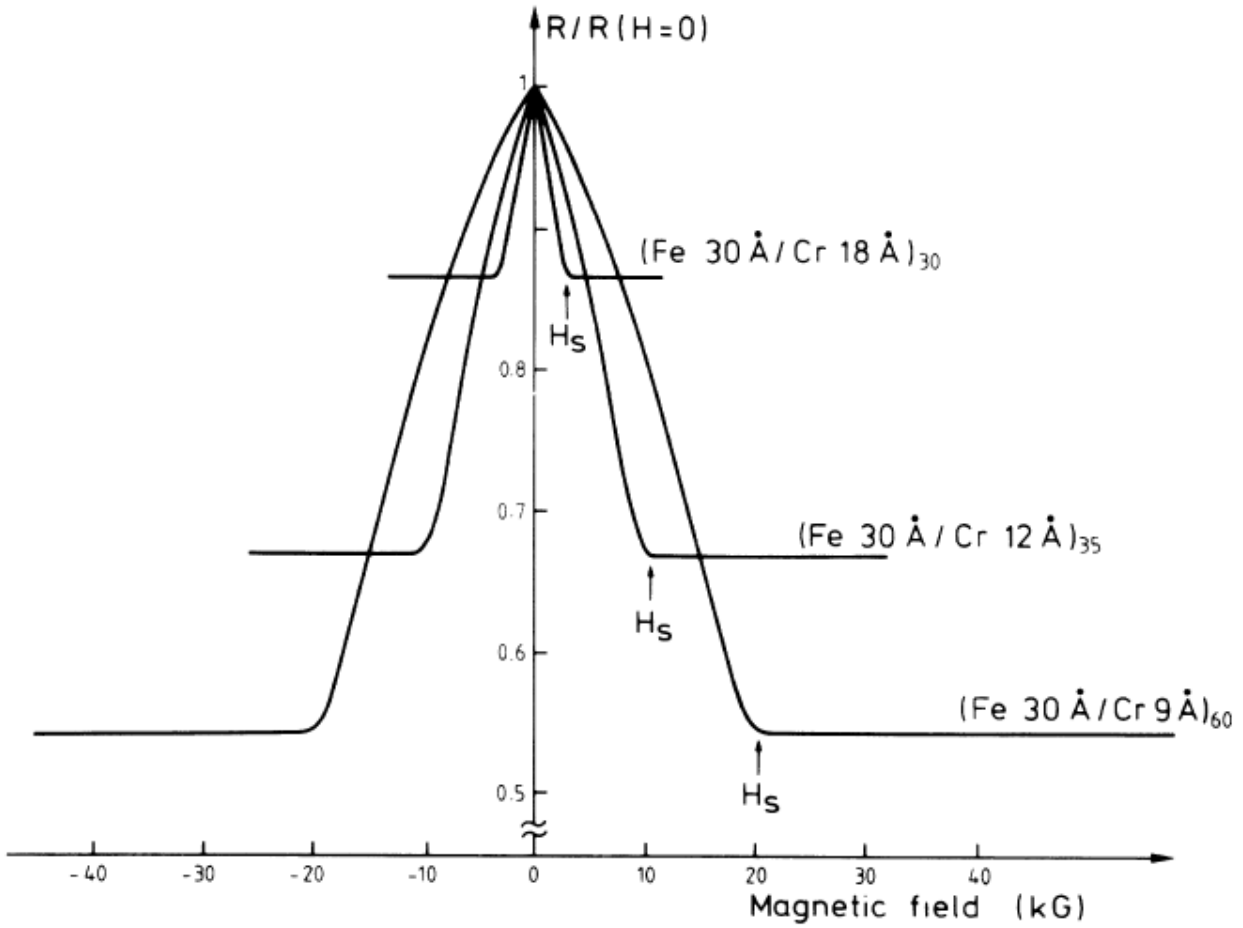

FIG. 3 Magnetoresistance of three Fe/Cr superlattices at 4.2 K. The current and the applied field are along the same [110] axis in the plane of the layers.

PRL 61, 2472 (1988):

In conclusion, we have found a giant magnetoresistance in (001)Fe/(001)Cr superlattices when, for thin Cr layers (9, 12, and 18 Å), there is an antiparallel coupling of the neighbor Fe layers at zero field. The highest magnetoresistance is observed in $[(\text{Fe } 30 \text{ Å})/(\text{Cr } 9 \text{ Å})]_{40}$: The resistivity is reduced by almost a factor of 2 when the magnetization is saturated. We interpret our results in terms of spin-dependent transmission between ferromagnetic layers. The giant magnetoresistance of the Fe/Cr superlattices may result from an interplay of the orientation of the Fe layers by an applied field with the spin-dependent transmission between Fe layers through a Cr layer. If one considers that strongly spin-dependent conduction occurs in many ferromagnetic transition-metal alloys,[11] the type of magnetoresistance found in Fe/Cr should be observed in other transition-metal superlattices. The existence of a giant magnetoresistance in Fe/Cr is promising for applications to magnetoresistance sensors. In the samples we have studied, the saturation fields are obviously too high for applications but a large magnetoresistance at relatively small fields can probably be obtained by thickening of the Fe layers (in a given field, this enhances the torque on the magnetic layers). Alternatively high magnetoresistance effects with weaker AF couplings should probably be observed with other couples of transition metals.

PRB 39, 4828 (1989):

RAPID COMMUNICATIONS

PHYSICAL REVIEW B VOLUME 39, NUMBER 7 1 MARCH 1989

Enhanced magnetoresistance in layered magnetic structures with antiferromagnetic interlayer exchange

G. Binasch, P. Grünberg, F. Saurenbach, and W. Zinn

Institut für Festkörperforschung, Kernforschungsanlage Jülich G.m.b.H., Postfach 1913, D-5170 Jülich, West Germany

(Received 31 May 1988; revised manuscript received 12 December 1988)

The electrical resistivity of Fe-Cr-Fe layers with antiferromagnetic interlayer exchange increases when the magnetizations of the Fe layers are aligned antiparallel. The effect is much stronger than the usual anisotropic magnetoresistance and further increases in structures with more than two Fe layers. It can be explained in terms of spin-flip scattering of conduction electrons caused by the antiparallel alignment of the magnetization.

PRB 39, 4828 (1989):

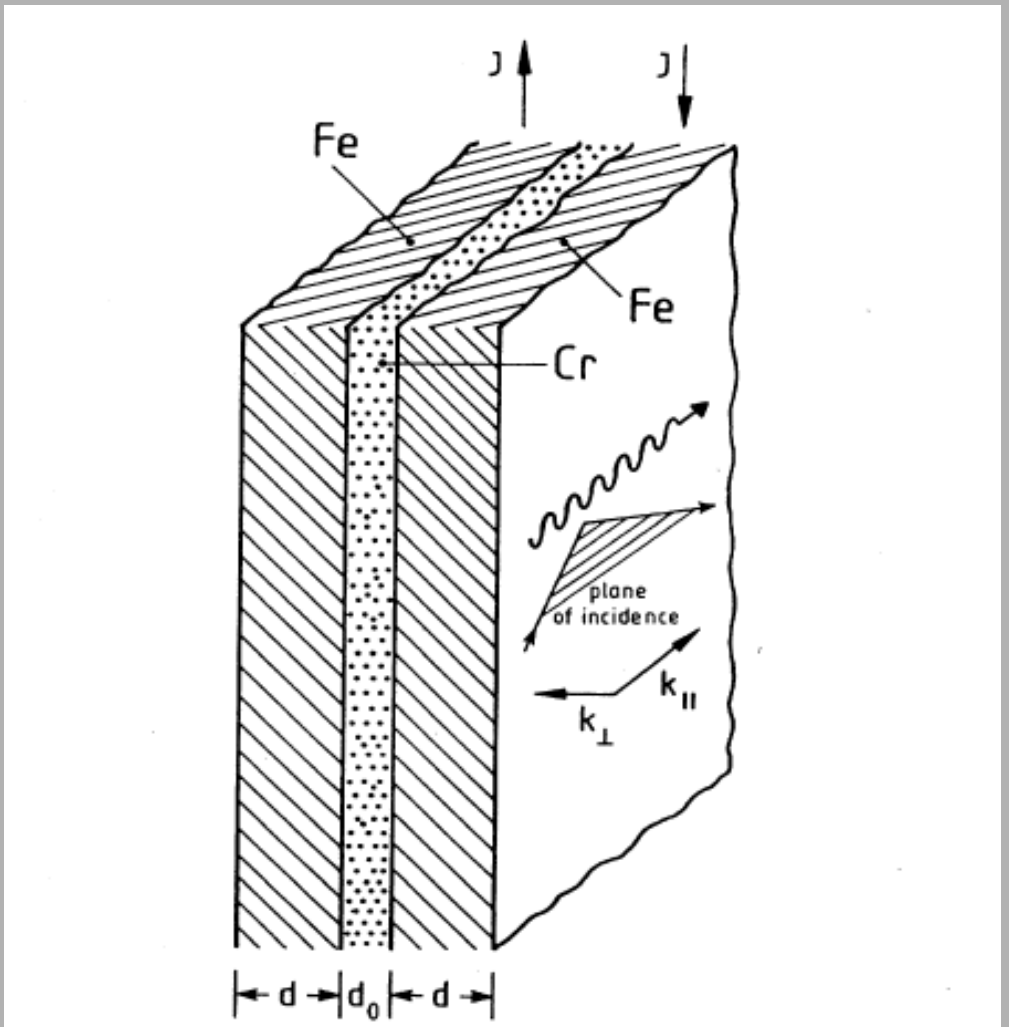

FIG. 1. Ferromagnetic double layer with antiparallel alignment of the magnetizations. Also indicated is the plane of incidence of the laser light for the observation of light scattering from spin waves and hysteresis curves via MOKE.

PRB 39, 4828 (1989):

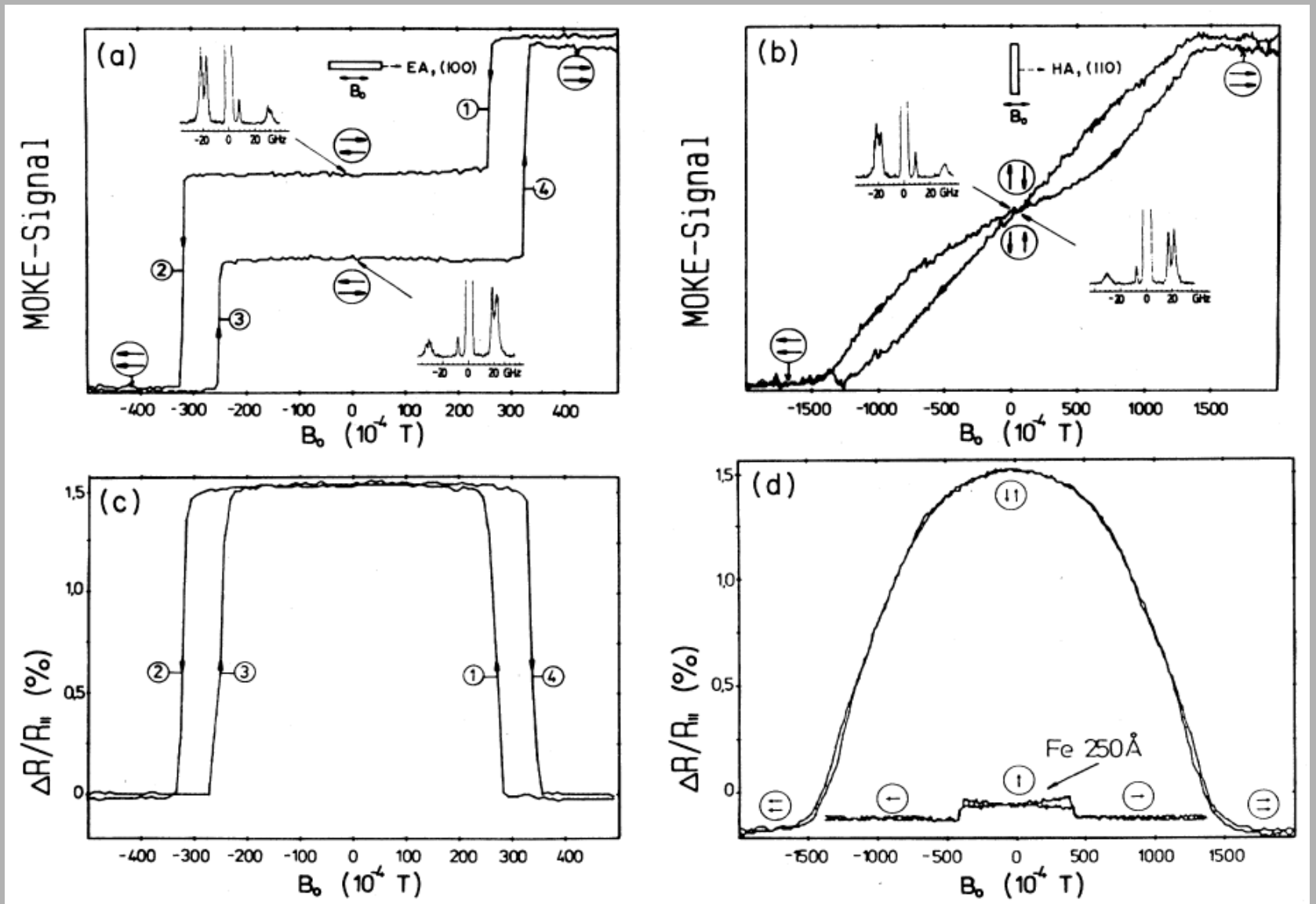

FIG. 2. (a)–(b) MOKE hysteresis curves and (c)–(d) magnetoresistance $\Delta R/R_{\parallel} = (R - R_{\parallel})/R_{\parallel}$ from Fe double layers with antiferromagnetic coupling. Also, (d) displays the anisotropic MR effect of a 250-Å-thick Fe film.

PRB 39, 4828 (1989):

We also have tested the possibility of a further increase of the effect by fabricating layered structures with more than two Fe films. In Fe trilayers with $d = 8$ nm and $d_0 = 1$ nm we obtained 3%, which doubles the effect seen in Fig. 2(d) from the double layers. Further increase to above 10% has been observed by cooling this sample to about 5 K.

For a quantitative analysis it would be important to know the mean free path for spin-flip scattering. It should be possible to obtain this information from the dependence of the effect on the thickness of the Fe films. Corresponding experiments are currently under way.

Note added. After submission of this manuscript it came to our knowledge that Baibich *et al.* have observed magnetoresistance changes as high as 50% at low temperatures in multilayered Fe-Cr structures.[10]

C:diamant a grafit

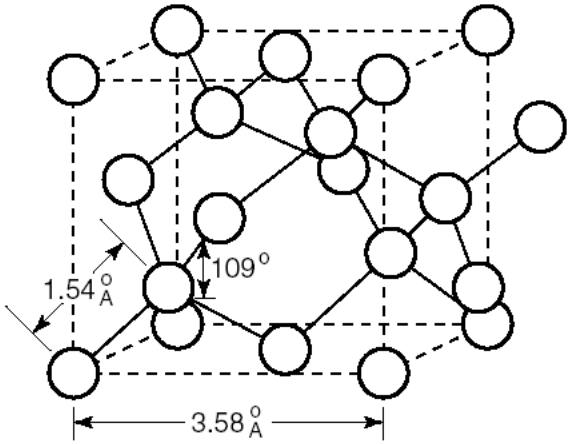

Figure 1-3. The crystal structure of diamond

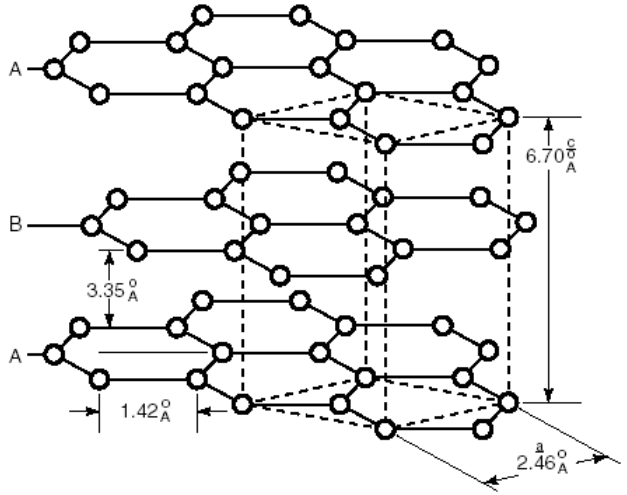

Figure 1-5.The crystal structure of graphite

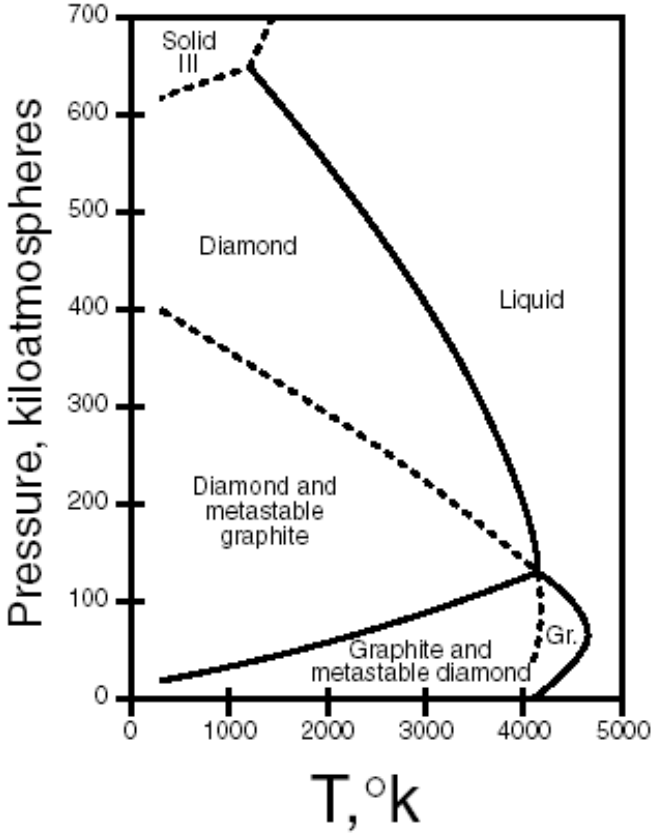

Figure 1-4. The carbon phase diagram

grafén

Electric Field Effect in Atomically Thin Carbon Films

K. S. Novoselov,[1] A. K. Geim,[1]* S. V. Morozov,[2] D. Jiang,[1] Y. Zhang,[1] S. V. Dubonos,[2] I. V. Grigorieva,[1] A. A. Firsov[2]

We describe monocrystalline graphitic films, which are a few atoms thick but are nonetheless stable under ambient conditions, metallic, and of remarkably high quality. The films are found to be a two-dimensional semimetal with a tiny overlap between valence and conductance bands, and they exhibit a strong ambipolar electric field effect such that electrons and holes in concentrations up to 10^{13} per square centimeter and with room-temperature mobilities of ~10,000 square centimeters per volt-second can be induced by applying gate voltage.

The ability to control electronic properties of a material by externally applied voltage is at the heart of modern electronics. In many cases, it is the electric field effect that allows one to vary the carrier concentration in a semiconductor device and, consequently, change an electric current through it. As the semiconductor industry is nearing the limits of performance improvements for the current technologies dominated by silicon, there is a constant search for new, nontraditional materials whose properties can be controlled by the electric field. The most notable recent examples of such materials are organic conductors (*1*) and carbon nanotubes (*2*). It has long been tempting to extend the use of the field effect to metals [e.g., to develop all-metallic transistors that could be scaled down to much smaller sizes and would consume less energy and operate at higher frequencies than traditional semiconducting devices (*3*)]. However, this would require atomically thin metal films, because the electric field is screened at extremely short distances (<1 nm) and bulk carrier concentrations in metals are large compared to the surface charge that can be induced by the field effect. Films so thin tend to be thermodynamically unstable, becoming discontinuous at thicknesses of several nanometers; so far, this has proved to be an insurmountable obstacle to metallic electronics, and no metal or semimetal has been shown to exhibit any notable (>1%) field effect (*4*).

We report the observation of the electric field effect in a naturally occurring two-dimensional (2D) material referred to as few-layer graphene (FLG). Graphene is the name given to a single layer of carbon atoms densely packed into a benzene-ring structure, and is widely used to describe properties of many carbon-based materials, including graphite, large fullerenes, nanotubes, etc. (e.g., carbon nanotubes are usually thought of as graphene sheets rolled up into nanometer-sized cylinders) (*5*–*7*). Planar graphene itself has been presumed not to exist in the free state, being unstable with respect to the formation of curved structures such as soot, fullerenes, and nanotubes (*5*–*14*).

[1]Department of Physics, University of Manchester, Manchester M13 9PL, UK. [2]Institute for Microelectronics Technology, 142432 Chernogolovka, Russia.

*To whom correspondence should be addressed. E-mail: geim@man.ac.uk

grafén

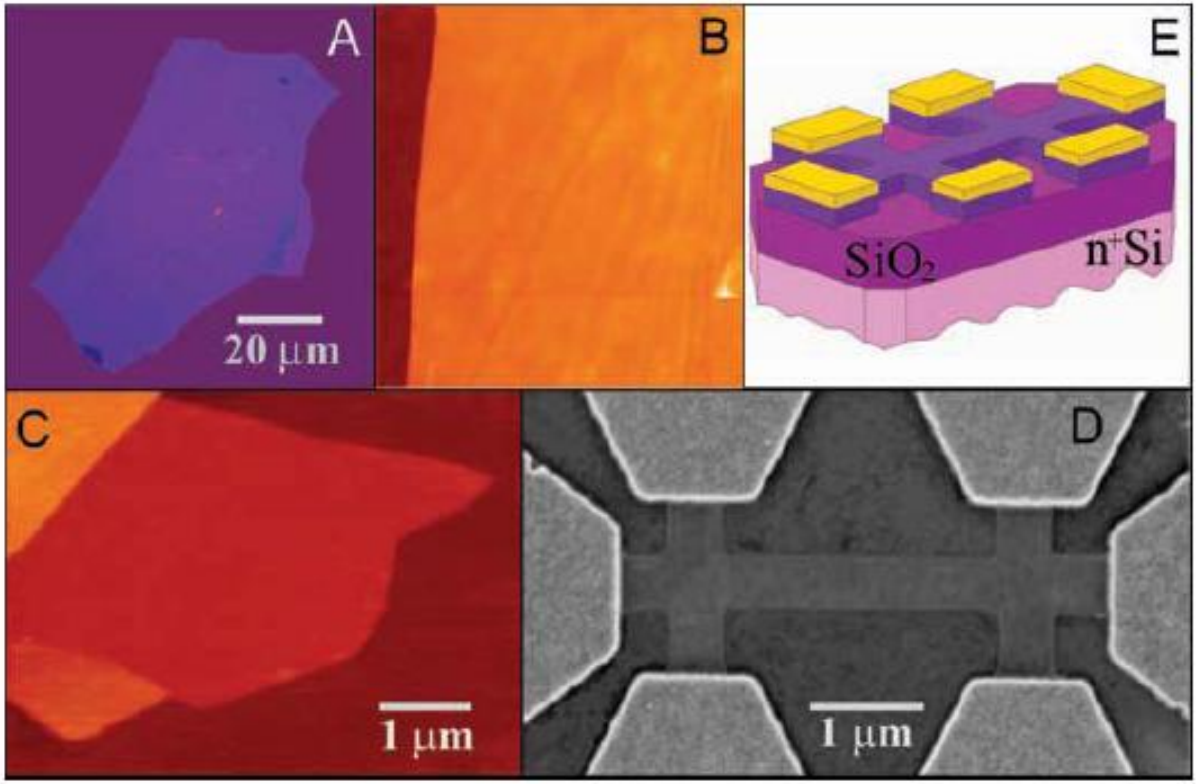

Fig. 1. Graphene films. (**A**) Photograph (in normal white light) of a relatively large multilayer graphene flake with thickness ~3 nm on top of an oxidized Si wafer. (**B**) Atomic force microscope (AFM) image of 2 μm by 2 μm area of this flake near its edge. Colors: dark brown, SiO_2 surface; orange, 3 nm height above the SiO_2 surface. (**C**) AFM image of single-layer graphene. Colors: dark brown, SiO_2 surface; brown-red (central area), 0.8 nm height; yellow-brown (bottom left), 1.2 nm; orange (top left), 2.5 nm. Notice the folded part of the film near the bottom, which exhibits a differential height of ~0.4 nm. For details of AFM imaging of single-layer graphene, see (*15*). (**D**) Scanning electron microscope image of one of our experimental devices prepared from FLG. (**E**) Schematic view of the device in (D).

Web of Science, “graphene”

1.10.2020 ... 234509 záznamů ; Citation Report feature not available

16.9.2019 ... 195139 záznamů ; Citation Report feature not available

18.9.2018 ... 160097 záznamů ; Citation Report feature not available

18.9.2017 ... 123080 záznamů ; Citation Report feature not available

24.9.2015 ... 69467, polovina roku 2009:

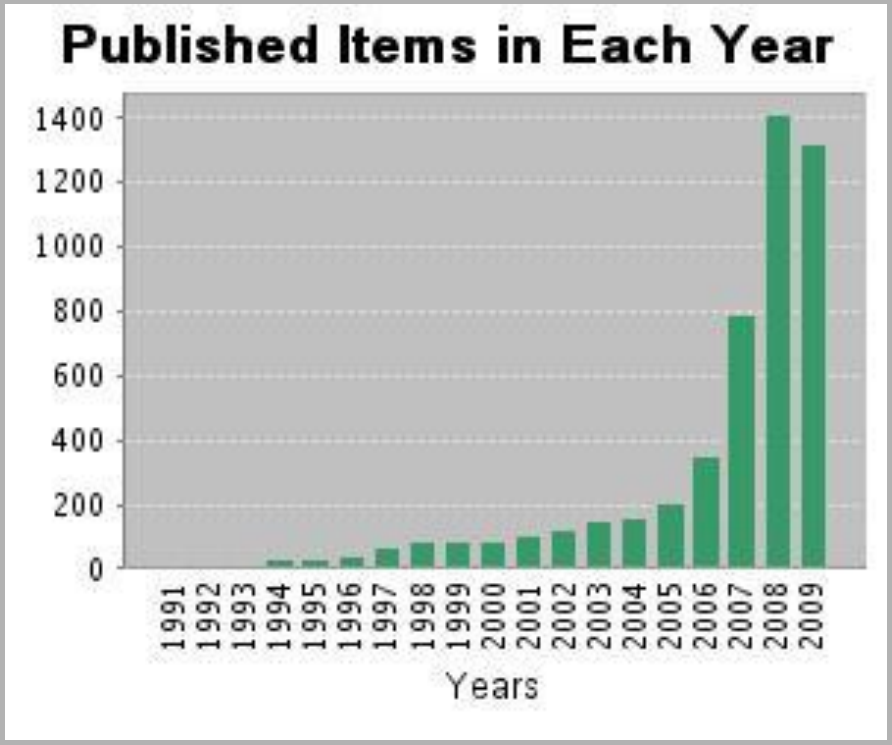

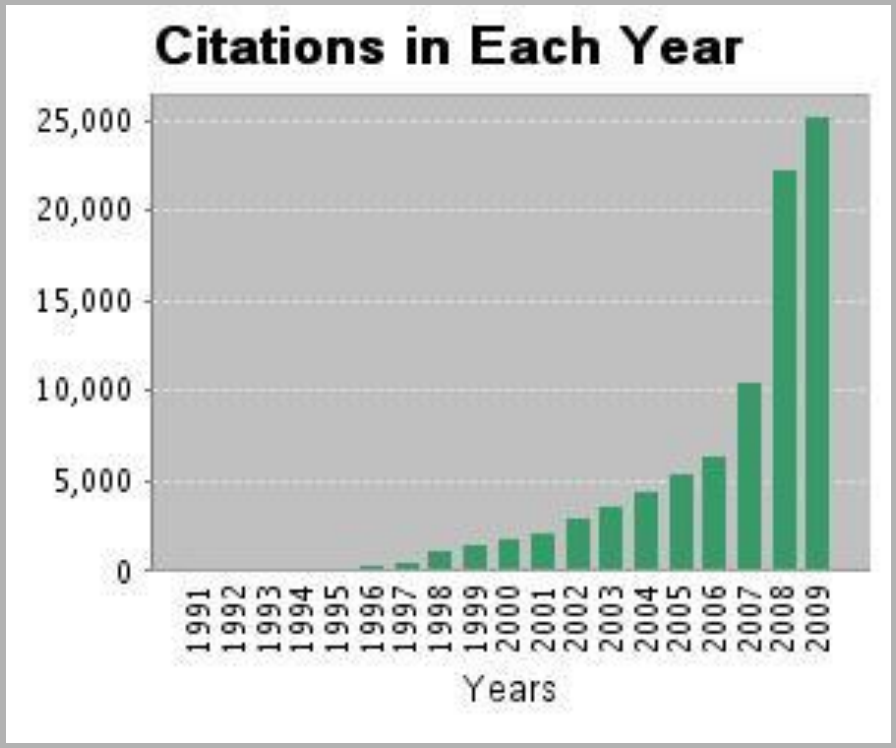

grafit: spektroskopie STM

Physica B 404 (2009) 2673–2677

Contents lists available at ScienceDirect

Physica B

journal homepage: www.elsevier.com/locate/physb

Electronic states on the surface of graphite

Guohong Li, Adina Luican, Eva Y. Andrei *

Department of Physics and Astronomy, Rutgers University, Piscataway, NJ 08854, USA

grafit: spektroskopie STM

ARTICLE INFO

Keywords:
Surfaces and interfaces
Scanning tunneling microscopy
Quantum Hall effect

ABSTRACT

Graphite consists of graphene layers in an AB (Bernal) stacking arrangement. The introduction of defects can reduce the coupling between the top graphene layers and the bulk crystal producing new electronic states that reflect the degree of coupling. We employ low temperature high magnetic field scanning tunneling microscopy (STM) and spectroscopy (STS) to access these states and study their evolution with the degree of coupling. STS in magnetic field directly probes the dimensionality of electronic states. Thus two-dimensional states produce a discrete series of Landau levels while three-dimensional states form Landau bands providing a clear distinction between completely decoupled top layers and ones that are coupled to the substrate. We show that the completely decoupled layers are characterized by a single sequence of Landau levels with square-root dependence on field and level index indicative of massless Dirac fermions. In contrast weakly coupled bilayers produce special sequences reflecting the degree of coupling, and multilayers produce sequences reflecting the coexistence of massless and massive Dirac fermions. In addition we show that the graphite surface is soft and that an STM tip can be quite invasive when brought too close to the surface and that there is a characteristic tip–sample distance beyond which the effect of sample–tip interaction is negligible.

grafit: spektroskopie STM, hrot Pt-Ir, mechanicky seříznutý

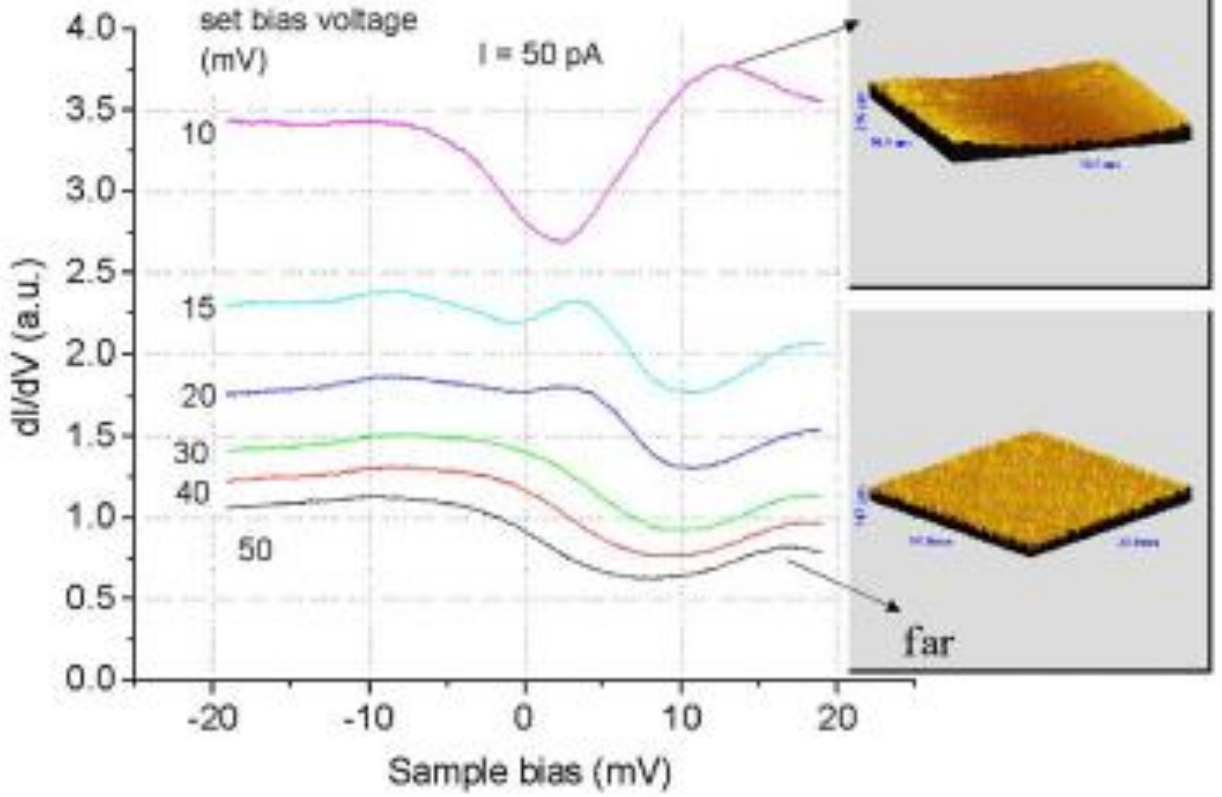

Fig. 1. Scanning tunneling spectroscopy for different tip–sample distance, which was controlled by the set bias voltage. Insets, STM images with size of 20 nm show a flat surface when the tip is far away from the sample surface but a dented one when the tip is near. Each spectrum was taken with ac modulation of 1 mV_{rms} and averaged over 256 spectra.

grafit: spektroskopie STM, hrot Pt-Ir, mechanicky seříznutý

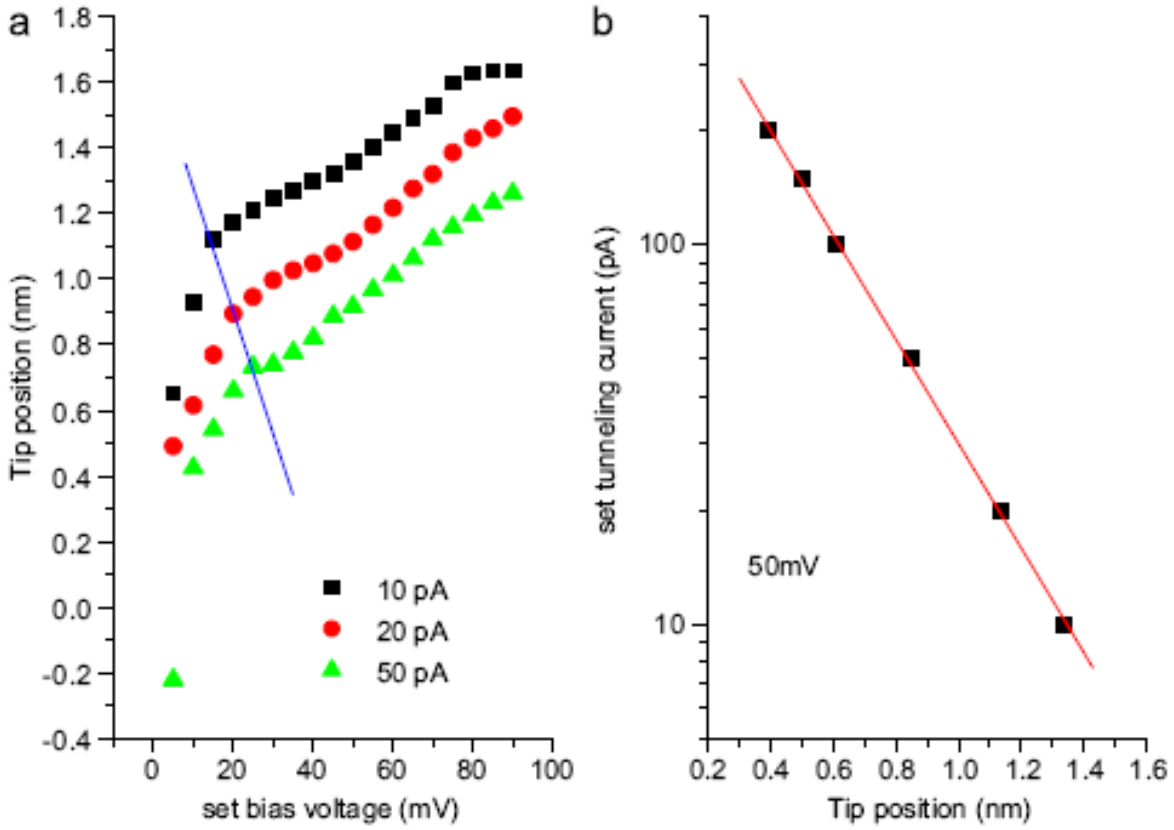

Fig. 2. (a) Tip position for different set tunneling currents for sample A. The line shows the onset of the low bias anomaly. (b) Tunneling current increases exponentially with decrease of tip–sample distance for set bias voltage of 50 mV.

grafit: spektroskopie STM, oddělené šupinky v magnet. poli

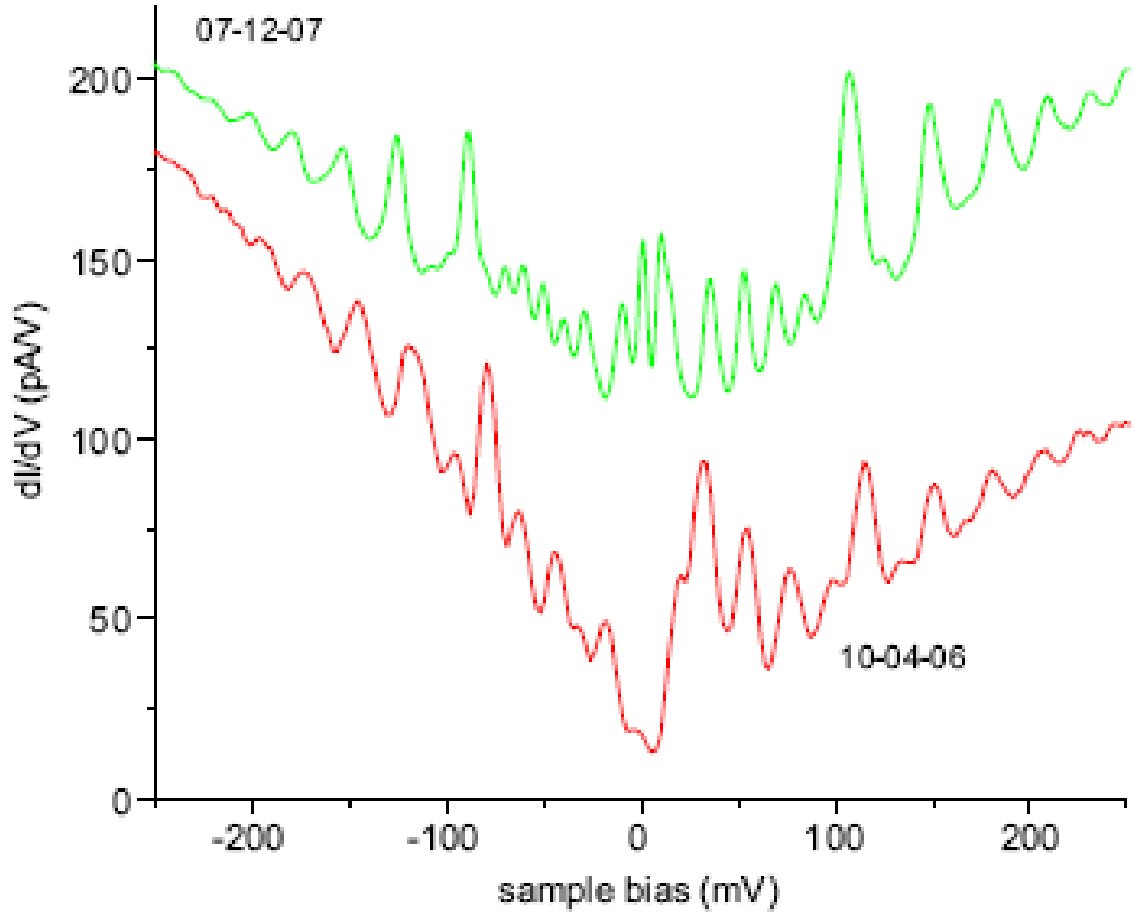

Fig. 6. Scanning tunneling spectroscopy of two samples in a field of 6 T. The spectra were shifted vertically for clarity.

témata:

- STM/AFM (princip, zajímavé obrázky)
- grafén (příprava vzorků, vlastnosti)

wikipedia, ...